Influence of the synergy between reaction, heat exchange and membrane separation on the process intensification of the dimethyl ether direct synthesis from carbon dioxide and hydrogen

Chakib R Behloul, Jean-Marc Jean-Marc.Commenge@univ-Lorraine.Fr Commenge, Christophe Castel

▶ **To cite this version:**

Chakib R Behloul, Jean-Marc Jean-Marc.Commenge@univ-Lorraine.Fr Commenge, Christophe Castel. Influence of the synergy between reaction, heat exchange and membrane separation on the process intensification of the dimethyl ether direct synthesis from carbon dioxide and hydrogen. Chemical Engineering and Processing: Process Intensification, 2021, 10.1016/j.cep.2021.108513 . hal-03413806

HAL Id: hal-03413806
https://hal.univ-lorraine.fr/hal-03413806

Submitted on 2 Aug 2023

HAL is a multi-disciplinary open access archive for the deposit and dissemination of scientific research documents, whether they are published or not. The documents may come from teaching and research institutions in France or abroad, or from public or private research centers.

L'archive ouverte pluridisciplinaire **HAL**, est destinée au dépôt et à la diffusion de documents scientifiques de niveau recherche, publiés ou non, émanant des établissements d'enseignement et de recherche français ou étrangers, des laboratoires publics ou privés.

Distributed under a Creative Commons Attribution - NonCommercial 4.0 International License

Version of Record: https://www.sciencedirect.com/science/article/pii/S0255270121002129
Manuscript_ca3a8bc495b3f57742050356007e50d2

Influence of the synergy between reaction, heat exchange and membrane separation on the process intensification of the dimethyl ether direct synthesis from carbon dioxide and hydrogen

Chakib R. Behloul[a,*], *Jean-Marc Commenge*[a], *Christophe Castel*[a]

[a] *Laboratoire Réactions et Génie des Procédés, UMR 7274, Université de Lorraine, CNRS, 1 rue Grandville, F-54000 Nancy, France*

[*] **Corresponding author: chakib-rafik.behloul@univ-lorraine.fr**

Highlights

- Process intensification by design of a multifunctional reactor.
- Approach based on characteristic times and dimensionless numbers.
- Minimization of the catalyst mass and hot spot intensity.
- Optimal conditions achieved due to a trade-off between these functions.
- Design of more compact equipment adapted to delocalized production.

ABSTRACT

© 2021 published by Elsevier. This manuscript is made available under the CC BY NC user license
https://creativecommons.org/licenses/by-nc/4.0/

This work presents a comprehensible approach based on the application of characteristic times and Damköhler numbers to optimize the synergy between catalytic reaction, heat exchange and membrane separation for an exothermic balanced reaction. This approach allows the description of parameters required to reduce limitations and intensify the process, considering the DME direct synthesis from a CO_2-rich feedstock as a case study. Different couplings are dealt with: reaction and heat exchange; reaction and separation; and reaction, heat exchange and separation. Coupling to a heat exchange enables to follow an optimal temperature progression and minimize the reactor volume by maximizing the reaction rate at any position, allowing the design of compact equipment adapted to delocalized production. Coupling to a membrane increases the achievable conversion at a given temperature. A trade-off between these functions is necessary to achieve the optimal conditions. Appropriate heat exchange enables proper membrane operation. Coupling to a separation improves the performance of a reactor-heat exchanger configuration. 85% of CO_2 conversion may be achieved. An optimization of the catalyst distribution is proposed, reducing the total catalyst mass by 21% and hot spot intensity by about 20 °C compared to a uniform catalyst distribution for an identical outlet conversion.

Keywords:

Process intensification

Dimensionless analysis

Heat transfer

Mass transfer

Reactor design

Membrane separation

NOMENCLATURE

a Interfacial area of heat transfer per unit reactor volume (m^2/m^3)

$\check{A}$ Total active membrane area (m^2)

$C_{p,i}$ Heat capacity at constant pressure of species i $(J/(mol.K))$

d_p Particle diameter (m)

$Da_{r,j}$ Reaction Damköhler number of reaction j

$Da_{r,j'}$ Reaction Damköhler number of key reaction j'

Da_t Thermal Damköhler number

Da_s Separative Damköhler number

D_{r_1} Internal reactor diameter (m)

D_{r_2} Shell reactor diameter (m)

e Membrane thickness (m)

$f_{i,ex}$ External resistance fraction

F_{tmb} Trans-membrane molar flow rate (mol/s)

$F_i^{*RZ(PZ)}$ Dimensionless molar flow rate of species i in the Reaction Zone (Permeation Zone)

i Species index

j Reaction index

j' Key reaction index

k_j Rate constant of the reaction j

K_{eq_j} Equilibrium constant of the reaction j

K_i Adsorption constant of the species i

L_{tot} Reactor tube length (m)

m_{cat} Catalyst mass (kg)

m Number of independent reactions

n Number of species

$n_{RZ(PZ)}$ Number of species in the Reaction Zone (Permeation Zone)

M Molecular weight (kg/mol)

P^{RZ} Total pressure in the Reaction Zone (Pa)

P_{H_2O} Water permeance $(mol/m^2.s.Pa)$

t_M Characteristic transfer time through the membrane (s)

t_Q Characteristic heat-transfer time (s)

t_R Characteristic reaction time (s)

T Temperature (K)

T_f Fluid coolant temperature (K)

r_j Rate of reaction j, $(mol/(kg.s))$

r_j^* Dimensionless rate of reaction j, $(mol/(kg.s))$

R Universal gas constant, $(J/(mol.K))$

$S_{H_2O/i}$ H_2O/i Membrane permselectivity

u_{in} Inlet superficial velocity of the fluid (m/s)

U Overall heat-exchange coefficient $(W/(m^2.K))$

$y_i^{*RZ(PZ)}$ Molar fraction of species i in the Reaction Zone (Permeation Zone)

z^* Dimensionless reactor length

Z Compressibility factor

ΔH_j Enthalpy of reaction j at temperature T (J/mol)

$\Delta H_{j'}$ Enthalpy of key reaction j' at temperature T (J/mol)

δ_j Pressure order related to the kinetic constant k_j

ε Porosity of the catalytic bed

κ_{H_2O} Water transfer coefficient through the membrane (m/s)

λ Thermal conductivity $(W/(m.K))$

μ Dynamic viscosity (Pa/s)

$\vartheta_{i,j}$ Stoichiometric coefficient of species i in reaction j

ρ_{app} Catalyst bed density (kg/m^3_{bed})

ρ_f Density of fluid (kg/m^3)

ρ_{f_0} Molar density (mol/m^3)

τ Residence time (s)

Φ Sweep flow rate ratio

ψ Pressure ratio

Ω Reactor cross section (m^2)

$GHSV$ Gas Hourly Space Velocity (h^{-1})

DME Di-Methyl Ether

LPG Liquefied Petroleum Gas

1. Introduction

According to the US Energy Information Administration [1] (EIA, 2020), the world's energy consumption will rise by nearly 50% between 2018 and 2050. The inability to attend that increase using conventional energy sources, such as fossil fuels, has made it important to discover new ways to produce energy. Similarly, the climate change and greenhouse gas emissions issue encourages the development of techniques to reduce the impact of these emissions while creating economic wealth and limit the global temperature increase to a given degree [2,3]. Carbone capture and storage technologies must be supported by its conversion into high value-added products in order to successfully limit its increase in the atmosphere [4,5,6,7,8,9]. Nearly all CO_2 emissions originate from fossil fuels, distributed among the

various sectors (transport, industry, heating, electricity, etc.). The power-to-fuel concept allows the synthesis of useful products for several purposes (fuel, petrochemical feedstock, etc.) through the CO_2 hydrogenation reaction [10]. The CO_2 hydrogenation opens the way for the introduction of renewable energies in the CO_2 recovery chain. The total cost of the process based on the CO_2 hydrogenation for the production of high value-added products depends strongly on the price and availability of hydrogen and its production method [11,12]. Moreover, with the generalization of the CO_2 environmental taxes, chemical industries are incited to restrict their CO_2 emissions and to use hydrogen obtained from intermittent carbon-free sources, in order to meet both environmental and economic requirements [13]. However, today's industries can benefit from the opportunities offered by the use of CO_2 as a raw material [3].

In this context, synthesis of methane (methanation), methanol, dimethyl ether (DME) and olefins from DME have in common that they are exothermic and balanced. These reactions, in addition to their exothermicity and thermodynamic equilibrium, are the subject of strong industrial demand for the distributed production and co-valorization of industrial carbon oxides and hydrogen from intermittent decarbonated sources. In addition, these reactions cover a wide range of cases in terms of enthalpies, operating conditions and technical, environmental and economic criteria (market scope, product selling price, etc.).

In this work, the DME direct synthesis from a CO_2-rich input mixture and hydrogen is considered as a case study. Industrial synthesis of DME has attracted attention in recent years due to these advantages and these different markets [14,15]: promoter alternative fuel for diesel vehicles with low emissions of NO_x, SO_x and harmful gases [16,17,18,19]; aerosol propellant [20,21]; similar characteristics to LPG in terms of physicochemical properties, handling and storage [22,23,24]; powering hydrogen-rich fuel cells [25,26]; petrochemical

filler for the synthesis of high value-added products (olefins, diethyl sulfate, etc.) [27,28,29,30].

Two methods are considered for the DME synthesis: the indirect and direct methods. Feasibility and economic advantages have led the researchers to prefer the direct synthesis in which methanol is formed and instantaneously converted to DME on a hybrid/ bifunctional catalyst (a mixture of metallic and acid functions: Cu-ZnO-Al_2O_3/δ-Al_2O_3 or HZSM-5, etc.) in the same reactor [31,32]. The process implemented to carry out the DME synthesis already shows a diversity of design configurations between reaction, heat exchange and separation pieces of equipment [33,34]. Similarly, different catalyst types have been proposed in the literature [23,35].

The DME direct synthesis from carbon oxides and hydrogen involves the consideration of the balanced following reactions:

$$CO_2 + 3H_2 \rightleftarrows CH_3OH + H_2O \quad ; \quad \Delta H_{298K} = -49.5\ kJ/mol \tag{1}$$

$$CO + 2H_2 \rightleftarrows CH_3OH \quad ; \quad \Delta H_{298K} = -90.7\ kJ/mol \tag{2}$$

$$2\ CH_3OH \rightleftarrows CH_3OCH_3 + H_2O \quad ; \quad \Delta H_{298K} = -23.5\ kJ/mol \tag{3}$$

$$CO_2 + H_2 \rightleftarrows CO + H_2O \quad ; \quad \Delta H_{298K} = +41.2\ kJ/mol \tag{4}$$

In this reaction system, there is a trade-off between kinetics and thermodynamics. The literature results, whether from simulation or experiment, have shown that the presence of CO_2 in the reactor feed is not in favor of the DME production [36,37,38]. This is mainly due to the water accumulation which has an adverse effect on both catalyst activity and methanol dehydration kinetics. The presence of excess water shifts the equilibrium in the opposite direction, reducing the production of the desired product and its selectivity. For these reasons, the call for intensification of the DME direct synthesis process is necessary to provide chemistry with the concept that will fulfill its needs.

Different techniques have been proposed in the literature for the water removal from the reaction zone, namely the water removal by sorption, or using a hydrophilic membrane or staged intercooling and condensation [39,40,41]. In this work, the coupling to a hydrophilic membrane will be preferred for water removal. The feasibility of membrane integration to enhance conventional processes has already been demonstrated in the literature for different reaction types at different operating conditions, for different purposes and in different ways [42,43,44,45,46,47,48,49,50]. In particular, the membrane types required in the DME direct synthesis for selective water removal are somehow specific: membranes must exhibit a certain thermal and mechanical stability, a high water selectivity and a high transmembrane flux. A family of hydrophilic inorganic membranes has been proposed in the literature and they have been well described in the works of Rohde et al. [51,52] and others [53,54,55]. These are mainly zeolite microporous, amorphous microporous and polymer membranes. These membranes differ in their synthesis method, structure, pore size, thickness, or transfer mechanism through the membrane, etc. Literature works [56,57,58] also reviewed different interesting points on this subject (results synthesis and comparison, membrane classification, etc.). According to these works, the zeolite microporous membrane is the favorite candidate to meet the criteria of their applicability in the DME direct synthesis [40,51,57,59,60]. Several kinds of zeolite membranes exist (Zeolite A, Chabazite, ZSM-5 and silicate-1 with MFI structure, Modernite, etc.) and they have been considered in several cases in the literature [42,61,62,63,64,65,66,67,68]. The ZSM-5/MFI membrane provides permeances in the range of 10^{-7}–10^{-6} mol/ (m^2 s Pa) and a permselectivity of water to hydrogen above 10 in temperature range [200-300] °C, which makes it suitable for the DME direct synthesis intensification [51]. Membrane integration enables improvement in reactor performance when applied in a one-step process, where the inhibition of methanol dehydration kinetics is

attenuated. Coupling to a membrane not only allows to shift the thermodynamic equilibrium but also ensures the catalyst activity by avoiding the crystallization of Cu and ZnO contained in the metallic catalyst and the loss of surface area, and ensures higher reaction rates by avoiding the decrease of reagents partial pressures by dilution [69].

Moreover, it is recognized that for this type of reaction, a high hot spot could be expected leading to catalyst deactivation or even reactor runaway [70,71,72]. However, due to both the exothermic nature and a thermodynamically limited conversion, and due to the harmful effects of the water presence in the reaction medium, simultaneous coupling to a heat exchanger and membrane separation is required. The integration of multiple functions within an equipment is a potential source of economic and energetic gains, especially when balanced exothermic reactions are intensified thanks to innovative coupling approaches [73].

The process intensification concept is in continuous evolution both in research and industrial fields [74,75,76]. In this context, the concept of multifunctional reactors, coupling several elementary functions is not a commonly-used approach, and their implementation did not become generalized due to a lack of manufacturing and design methodology [73]. The rise of numerical simulation tools has allowed their development on a case-by-case basis, to the detriment of general engineering methods based on the characteristic properties of the systems under consideration. Generally, to deal with such a process problem, a question should be asked: what is the proper strategy to intensify and for which problem? A possible way to answer this question consists in analyzing the system limitations. According to the previous description, three limitations can be identified at least: limitation by transfer, limitation by a thermodynamic equilibrium and a limitation by a risk related to the process exothermicity.

To address this point, the present work will discuss an approach that has not been reported in the literature for the DME direct synthesis from a CO_2-rich feedstock and H_2. This

approach is based on the use of characteristic times and dimensionless numbers for different purposes : (i) to quantify the impact of couplings on the performance of the synthesis, with a view to targeting intensification strategies that will take advantage of their synergies; (ii) to identify the sensitivity of reaction, heat-transfer and transmembrane permeation rates on the reactor performance; (iii) to establish the appropriate ranges in which mass and heat transfer coupling is/are required to intensify the process; and (iv) to define a comprehensible approach of compact reactor sizing from the limitations identification.

2. Modeling and simulation

2.1 Method overview

Fig. 1 presents an overview of the considered approach. Among the set of possible limitations, the identification of process limitations by characteristic time analysis will help the choice and design of a specific equipment.

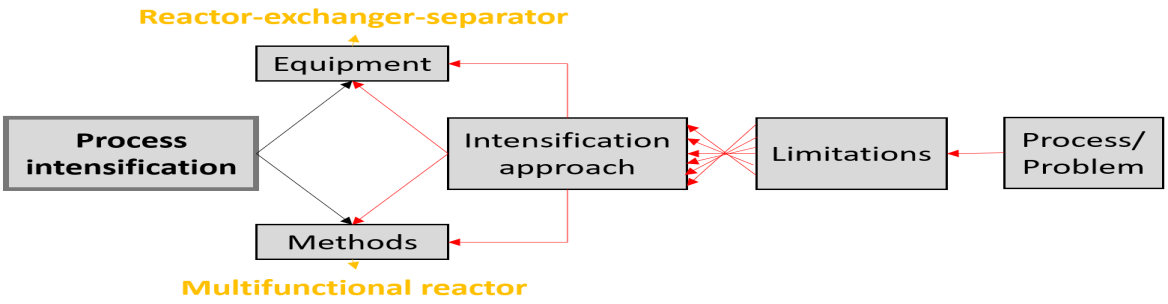

Fig. 1. Schematic representation of the considered approach.

Analysis of characteristic times allows to compare the fundamental phenomena to the operating parameters imposed by the process operating conditions. The comparison of these fundamental characteristic times makes possible to identify the limiting phenomenon and to define design or sizing strategies aiming at removing this limitation. The characteristic time of a phenomenon is a measure of its own rate: a low characteristic time indicates a fast phenomenon and conversely. Using this approach allows to gather the various phenomena affecting the reactor performance on a single scale: the time scale. Moreover, the ratio of two

characteristic times provides a dimensionless number, and these numbers characterize the different transport phenomena and their competitions within the reactor (mass transfer, heat transfer, convective transport). A good understanding of these characteristic times leads to the definition of an approach for the design of an intensified reactor enables to remove selectively the limitations that reduce the reactor performances.

2.2 Independence of reactions

For a global approach, the number of independent reactions can be obtained by a simplified method suggested in the literature [77], mainly based on the following principle: in a system with m' reactions and n species with stoichiometric coefficients $\vartheta_{i,j}$ $(1 \leq i \leq n; 1 \leq j \leq m')$ a sub-matrix $(A_{m,n})$ with as many rows $(m \leq m')$ as possible has to be derived from the main matrix of stoichiometric coefficients $(A_{m',n})$ for an identical number of columns (species number), so that no coefficient $(\vartheta_{j'})$ can be found satisfying the following condition (equation (5)):

$$\sum_{j=1}^{m} \vartheta_{j'} \, \vartheta_{i,j} = 0 \tag{5}$$

The principle is to convert the main matrix $(A_{m',n})$ into a step matrix (reduced step). The number of rows not completely filled with zeros of this stepped matrix corresponds to the independent reactions number (m). Once the number (m) is identified, all the other rows are just a linear combination of the other reactions. The final choice of independent reactions differs from one model to another, which is also the case for the DME direct synthesis. The number of the independent reactions is reported in the literature for the DME direct synthesis: it is equal to 3.

In this work, the Nie et al. [78] model, based on the Langmuir-Hinshelwood mechanism, considers the first three reactions (equations (1), (2) and (3)) described above, and the reaction rates expressions are given as follows:

$$r_1 = \frac{k_1 f_{CO_2} f_{H_2}^3 \left(1 - \frac{f_{CH_3OH} f_{H_2O}}{K_{eq_1} f_{CO_2} f_{H_2}^3}\right)}{\left(1 + K_{CO_2} f_{CO_2} + K_{CO} f_{CO} + K_{H_2} f_{H_2}\right)^4}$$

$$r_2 = \frac{k_2 f_{CO} f_{H_2}^2 \left(1 - \frac{f_{CH_3OH}}{K_{eq_2} f_{CO} f_{H_2}^2}\right)}{\left(1 + K_{CO_2} f_{CO_2} + K_{CO} f_{CO} + K_{H_2} f_{H_2}\right)^3}$$

$$r_3 = \frac{k_3 f_{CH_3OH} \left(1 - \frac{f_{DME} f_{H_2O}}{K_{eq_3} f_{CH_3OH}^2}\right)}{\left(1 + \sqrt{K_{CH_3OH} f_{CH_3OH}}\right)^2}$$

The kinetic parameters of this model as well as the equilibrium constants considered are presented in **Table 1** and **Table 2**. The choice of this model has previously been detailed [73].

Table 1
Kinetic parameters for the considered model [78].

Parameter	Expression	Unit
k_1	$1.4053 * 10^{-17}\ exp(-67515/RT)$	$mol/kg\ s\ Pa^4$
k_2	$2.05 * 10^{-12}\ exp(-54307/RT)$	$mol/kg\ s\ Pa^3$
k_3	$2.95 * 10^{-3}\ exp(-43473/RT)$	$mol/kg\ s\ Pa$
K_{CO}	$3.934 * 10^{-11}\ exp(37373/RT)$	Pa^{-1}
K_{CO_2}	$1.858 * 10^{-11}\ exp(53795/RT)$	Pa^{-1}
K_{H_2}	$0.6716 * 10^{-5}\ exp(-6476/RT)$	Pa^{-1}
K_{CH_3OH}	$3.48 * 10^{-11}\ exp(54689/RT)$	Pa^{-1}

Table 2
Correlations for equilibrium constant calculations [70,79,80].

Reaction	Expression	Unit
$CO_2\ hydrogenation$	$Log_{10} K_{eq1} = \frac{3066}{T} - 10.592$	bar^{-2}
$CO\ hydrogenation$	$Log_{10} K_{eq2} = \frac{5139}{T} - 12.621$	bar^{-2}
$Methanol\ dehydration$	$ln\ K_{eq3} = \frac{4019}{T} + 3.707\ ln(T) - 2.783 * 10^{-3}\ (T) + 3.8 * 10^{-7}\ (T^2)$ $-6.561 * 10^4\ (T^{-3}) - 26.64$	–

2.3 Reactor configuration

The schematic reactor configuration proposed in this work is shown in **Fig. 2**. The proposed reactor consists of two coaxial tubes. For mechanical stability reasons and easy handling of the ratio between catalyst mass and membrane area, the inner tube corresponds to the

membrane and is surrounded by the reaction zone. Under the driving force influence, the produced water is forced to leave the reaction zone (RZ) towards the permeation zone (PZ).

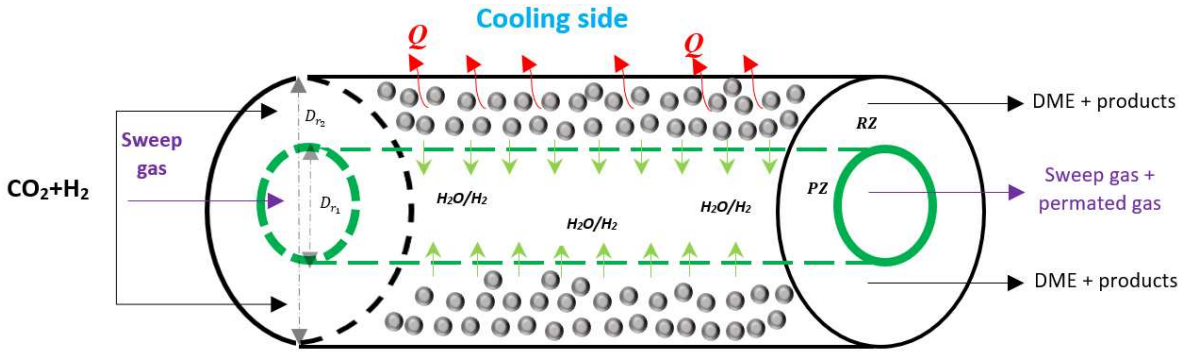

Fig. 2. Schematic view of the considered multifunctional reactor configuration.

A sweep gas (N_2) flows through the inner tube in co-current with respect to the feed in order to carry the permeated gas outside the permeation zone and/or to keep the partial pressure of the permeated gas as low as possible. The annular space between the two tubes refers to the reaction zone where the catalytic particles for the DME direct synthesis are packed. A heat-transfer fluid surrounds the second tube to remove the heat generated in the reaction zone due to the exothermic nature of the global process. As the effect of the membrane thickness is included in the permeance factor, for simplification reasons, an overall internal diameter D_{r_1} is considered in the balance equations. The transmembrane molar flux for species i, described by equation (6), is defined as the product of a driving force through the membrane (partial pressure difference) and the membrane specific properties (permeance $\mathcal{P}_i$ and total active area $\check{A}$). In this work, only water and hydrogen can permeate through the membrane in order to evaluate the influence of the interaction between reaction, heat exchange and quasi-real zeolite membrane separation on the process intensification of the dimethyl ether direct synthesis from CO_2-rich input mixture.

$$F_{tmb,i} = \check{A}\, \mathcal{P}_i\, P^{RZ} \left(y_i^{RZ} - y_i^{PZ} \frac{P^{PZ}}{P^{RZ}} \right) \tag{6}$$

The considered reactor model is based on the following assumptions: (a) 1D plug-flow pseudo-homogeneous reactor; (b) steady state and negligible pressure drop along both reaction and permeation zones; (c) due to a reactor ratio Length/Diameter over 50, the radial gradients are neglected at any given axial position; (d) due to the chosen catalyst particle size and solid conductivity, internal transfer resistances may be neglected; (e) the membrane exhibits no resistance to heat transfer (temperatures in both reaction and permeation zones are equal).

The external mass transfer can also be neglected after post-processing verification of the value of the external resistance fraction ($f_{i,ex} << 1$) [81] or the Mears' criterion computation (Mc<0.15) [82]. Hydrocarbon production is not considered in this paper.

2.4 Dimensionless heat and mass transfer balances

The heat and mass balance equations will be expressed as a function of the dimensionless numbers described below, making it possible to both exploit the wide range of operating conditions and to better understand the coupling between reaction, heat exchange and separation. These dimensionless numbers characterize the different transport phenomena within the reactor (mass transfer, heat transfer, convective transport). The mass balances in the reaction zone and in the permeation zone are described respectively by equations (7) and (8). In order to make it easier for the readers to interpret the temperature profile (heat distribution) within the reactor, the heat balance will include the dimensionless numbers as well, but is kept in dimensional temperature. Otherwise, one can easily make the heat balance totally dimensionless by taking $T^* = T/T_{in} - 1$ and $T_f^* = T_f/T_{in} - 1$. The energy balance is given by equation (9).

$$\frac{dF_i^{*RZ}}{dz^*} = Da_{r,j'}\left[\sum_{j=1}^{m} \vartheta_{i,j}\, r_j^*\, K_{j,j'} - \frac{Da_s}{Da_{r,j'}}\frac{1}{S_{H_2O/i}}\left(y_i^{*RZ} - \psi\, y_i^{*PZ}\right)\right];\ (1 \le i \le n) \qquad (7)$$

$$\frac{dF_i^{*PZ}}{dz^*} = Da_{r,j'}\left[\frac{Da_s}{Da_{r,j'}}\frac{1}{\Phi}\frac{1}{S_{H_2O/i}}\left(y_i^{*RZ} - \psi\, y_i^{*PZ}\right)\right];\ (1 \le i \le n) \tag{8}$$

$$\frac{dT}{dz^*} = Da_{r,j'}\left[\frac{\sum_{j=1}^{m}\left(-\Delta H_{j'}\right) r_j^*\, H_{j,j'}\, K_{j,j'}}{\widetilde{FCp}} - \frac{Da_t}{Da_{r,j'}}\left(T - T_f\right)\right] \tag{9}$$

Where i denotes the species index (CO_2, CH_3OH, CO, H_2, H_2O, DME, inert), j denotes the reaction index $(1 \le j \le m)$ and j' denotes the key reaction (methanol dehydration to DME, equation (3)). In these equations, $\vartheta_{i,j}$ denotes the stoichiometric coefficient of species i in reaction j, $\Delta H_{j'}$ is the enthalpy of key reaction j' at temperature T, T is the local temperature, T_f is the coolant temperature, Cp_i is the heat capacity of species i at constant pressure, $r_j^* = r_j/k_j P^{\delta_j}$ is the dimensionless rate of reaction j, δ_j is the pressure order related to the kinetic constant k_j. $F_i^{*RZ(PZ)} = F_i^{RZ(PZ)}/F_{in}^{RZ(PZ)}$ is the dimensionless molar flow rate, $z^* = z/L_{tot}$ is the dimensionless position along the reactor, $\widetilde{FCp} = \sum_{i=1}^{n_{RZ}} F_i^* Cp_i + \sum_{i=1}^{n_{PZ}} F_i^* Cp_i$. All other parameters are described in **Table 3** with the definition of each dimensionless number.

Table 3
Set of governing dimensionless numbers for the considered model.

Notation	Parameter	Expression	Definition/Ratio
$Da_{r,j}$	Reaction Damköhler number	$Da_{r,j} = k_j P^{\delta_j} \rho_{app} \frac{R\, T_{in}}{P_{in}^{RZ}} \frac{L_{tot}}{u_{in}}$	$\frac{\text{Residence time } (\tau)}{\text{Characteristic reaction time } (t_R)}$
Da_s	Separative Damköhler number	$Da_s = \mathcal{P}_{H_2O} P^{RZ} \frac{R\, T_{in}}{P_{in}^{RZ}} \frac{\pi D_{r_1}}{\Omega} \frac{L_{tot}}{u_{in}}$ $Da_s = \kappa_{H_2O} \frac{P^{RZ}}{P_{in}^{RZ}} \frac{\pi D_{r_1}}{\Omega} \frac{L_{tot}}{u_{in}}$	$\frac{\text{Residence time } (\tau)}{\text{Characteristic membrane transfer time } (t_M)}$
Da_t	Thermal Damköhler number	$Da_t = \frac{U\, a}{\rho_{f_0} \widetilde{FCp}} \frac{L_{tot}}{u_{in}}$	$\frac{\text{Residence time } (\tau)}{\text{Characteristic heat} - \text{transfer time } (t_Q)}$
$S_{H_2O/i}$	Membrane permselectivity	$S_{H_2O/i} = \frac{\mathcal{P}_{H_2O}}{\mathcal{P}_i}$	$\frac{\text{Water permeance}}{\text{Permeance of species i}}$
ψ	Pressure ratio	$\psi = \frac{P^{PZ}}{P^{RZ}}$	$\frac{\text{Total pressure in permeation zone}}{\text{Total pressure in reaction zone}}$
Φ	Sweep flow rate ratio	$\Phi = \frac{F_{in}^{PZ}}{F_{in}^{RZ}}$	$\frac{\text{Molar inlet flow rate of sweep gas}}{\text{Molar inlet flow rate on the reaction zone}}$
$K_{j,j'}$	Reaction Damköhler ratio	$K_{j,j'} = \frac{Da_{r,j}}{Da_{r,j'}} = \frac{k_j P^{\delta_j}}{k_{j'} P^{\delta_{j'}}}$	$\frac{\text{Damköhler related to reaction j}}{\text{Damköhler related to key reaction j'}}$

$H_{j,j'}$	Enthalpy ratio	$H_{j,j'} = \frac{\Delta H_j}{\Delta H_{j'}}$	$\frac{\text{Enthalpy of reaction j}}{\text{Enthalpy of key reaction j'}}$
$\frac{Da_s}{Da_{r,j}}$	Damköhler ratio (separation-reaction)	$\frac{Da_s}{Da_{r,j}} = \frac{\mathcal{P}_{H_2O}\, P^{RZ}}{k_j P^{\delta_j}\, \rho_{app}} \frac{\pi D_{r_1}}{\Omega}$	$\frac{\text{Characteristic reaction time } (t_R)}{\text{Characteristic membrane transfer time } (t_M)}$
$\frac{Da_t}{Da_{r,j}}$	Damköhler ratio (heat exchange-reaction)	$\frac{Da_t}{Da_{r,j}} = \frac{U\, a}{k_j P^{\delta_j}\, \rho_{app}} \frac{1}{\widetilde{FCp}}$	$\frac{\text{Characteristic reaction time } (t_R)}{\text{Characteristic heat} - \text{transfer time } (t_Q)}$

Where ε is the catalytic bed porosity, L_{tot} is the reactor length, u_{in} is the inlet superficial velocity, ρ_{app} is the catalyst bed density, k_j is the kinetic constant of reaction j, δ_j is the pressure order related to the kinetic constant k_j, $\Omega = \pi\left(D_{r_2}^2 - D_{r_1}^2\right)/4$ is the cross section of the reaction zone, $\kappa_{H_2O} = \mathcal{P}_{H_2O} R\, T_{in}$ is the water transfer coefficient through the membrane, $\mathcal{P}_{H_2O}$ is the water permeance, ρ_{f_0} is the inlet molar density in the reaction zone, U is the overall heat-transfer coefficient and $a = 4\, D_{r_2}/\left(D_{r_2}^2 - D_{r_1}^2\right)$ is the interfacial area of heat transfer per unit reactor volume.

The residence time is related to the reactor inlet conditions, and is involved in the three Damköhler dimensionless numbers, in which it is compared to the suitable characteristic time. A characteristic time informs on the phenomenon rate: a phenomenon is as fast as its characteristic time is low and inversely [83]. In order to get used to these dimensionless numbers, a high Da_t means a high heat-transfer rate, and a low Da_s means a small permeation rate through the membrane. The membrane reactor behaves like a conventional reactor without membrane at very low Da_s values. In order to avoid repetitive parts in the present work and to properly interpret the results, detailed explanations of the physical meaning of the characteristic times will be given further in the paper.

Table 4 shows the explicit definition of these ratios of dimensionless numbers and how the transfer phenomena rates can be affected by the design parameters and operating conditions.

Table 4
Explicit definition of dimensionless number ratios.

Parameter	Design parameter	Reaction process conditions

$\frac{Da_s}{Da_{r,j}}$	$\frac{4\ D_{r_1}}{D_{r_2}^2 - D_{r_1}^2}\Upsilon_{H_2O}$	$\frac{P^{RZ}}{k_j P^{\delta_j}\ \rho_{app}}$
$\frac{Da_t}{Da_{r,j}}$	$U\ a$	$\frac{1}{k_j P^{\delta_j}\ \rho_{app}\ \widetilde{FCp}}$

Table 4 shows that diameter, permeance (including membrane thickness) and heat-transfer parameters influence the transfer rates (characteristic times), and should allow, through their parameterization, the design of more efficient compact reactors.

The described balances can be adapted in the simulation part according to the type of coupling, coupling 'reaction-heat exchange' (R-E), coupling 'reaction-separation' (R-S) and coupling 'reaction-heat exchange-separation' (R-E-S) as follows:

$$R - E \rightarrow Da_s = 0, y_{in}^{PZ} = 0$$
$$R - S \rightarrow Da_t = \infty$$
$$R - E - S \rightarrow Da_{r,j'} \neq 0, Da_s \neq 0, Da_t \geq 0.$$

The heat exchange modes can be managed as follows:

$$Isothermal \rightarrow Da_t = \infty$$
$$Adiabatic \rightarrow Da_t = 0$$
$$Isoperibolic \rightarrow Da_t \neq 0.$$

The inlet boundary conditions are:

$$F_i^{*RZ\ (PZ)}(z^* = 0) = y_{i,in}^{RZ\ (PZ)}$$
$$P^{(RZ)}(z^* = 0) = P_{in}$$
$$P^{(PZ)}(z^* = 0) = \psi\ P_{in}$$
$$T(z^* = 0) = T_{in}$$

The total molar flow rates in the two zones and the partial pressures are updated at each axial position. The correlations allowing the calculation of the various parameters and properties of the gaseous mixture (compressibility factor Z, heat capacity Cp, density ρ, viscosity μ, average molecular weight M, etc.) are reported in **Supporting Information**.

All the balance differential equations have been implemented in MATLAB R2019b. The 'ode15s' solver, adapted to stiff systems, has been used to integrate the reactor. For accuracy reasons, the relative and absolute tolerances are set respectively at 10^{-8} and 10^{-6}.

The reactor properties and the operating conditions considered are summarized in **Table 5**.

Table 5
Reactor geometry, operating conditions.

Parameter	Value	Unit
D_{r_1}	1.4	cm
D_{r_2}	2.5	cm
ε	0.42	–
d_p	2	mm
T_{in}	250	$°C$
P_{in}	5	MPa
ψ	0.2 – 0.8	–
Φ	1 – 10	–
H_2/CO_2	3	–
CO_2/CO	8	–

CO_X and CO_2 conversions, the DME yield and DME selectivity are given as follows (equations (10), (11), (12) and (13)):

$$X_{CO_X} = 1 - \frac{(F_{CO_2}+F_{CO})_{out}}{(F_{CO_2}+F_{CO})_{in}} \quad (10)$$

$$X_{CO_2} = 1 - \frac{(F_{CO_2})_{out}}{(F_{CO_2})_{in}} \quad (11)$$

$$y_{DME} = \frac{(2F_{DME})_{out}}{(F_{CO_2}+F_{CO})_{in}} \quad (12)$$

$$S_{DME} = \frac{(2F_{DME})_{out}}{(2F_{DME})_{out}+(F_{CH_3OH})_{out}} \quad (13)$$

3. Results and discussion

In order to get insight and to understand the effect of each of the dimensionless numbers (coupling effect) on the simulation results, some preliminary results are presented in **Fig. 3** and **Fig. 4**.

Fig. 3 shows the Damköhler numbers effect on the CO_2 and H_2 dimensionless flow rate evolution. In **Fig. 3**a and **Fig. 3**c, the smaller the characteristic reaction time (higher key reaction Damköhler $Da_{r,j'}$), the faster the kinetics at the reactor inlet: this is reflected by various initial slopes.

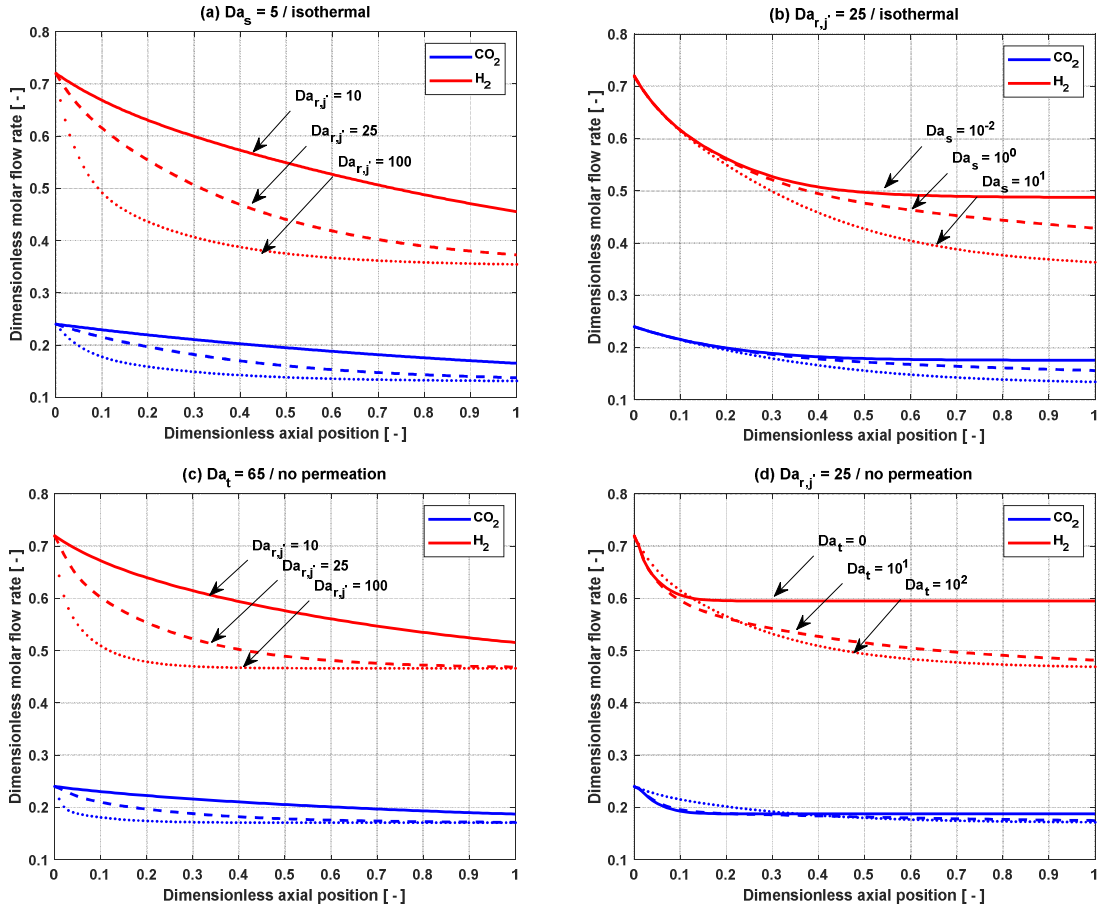

Fig. 3. Dimensionless molar flow rate evolutions of CO_2 and H_2 along the reactor. ($S_{H_2O/H_2} = \infty$, $\psi = 0.8$ and $\Phi = 1$)

In **Fig. 3**b, coupling to a membrane ($Da_s > 0$) breaks the thermodynamic equilibrium barrier, leading to a higher reagent conversion at the reactor outlet. As the characteristic transfer time through the membrane increases (Da_s decreases), the reactor behavior approaches that of a conventional reactor. In **Fig. 3**d, the initial slope of the profile at low Da_t merges with the initial slope of the profile under adiabatic conditions ($Da_t = 0$). This means that the heat generation time (characteristic reaction time) is very small compared to the characteristic heat-transfer time. Increasing the Da_t improves the heat-exchange quality by efficiently removing the reaction's heat.

Fig. 4 shows a generalized view of the results presentation in the (T; X) path for different couplings. **Fig. 4**a and **Fig. 4**b illustrate respectively the impact of coupling to a heat exchange and to a membrane separation.

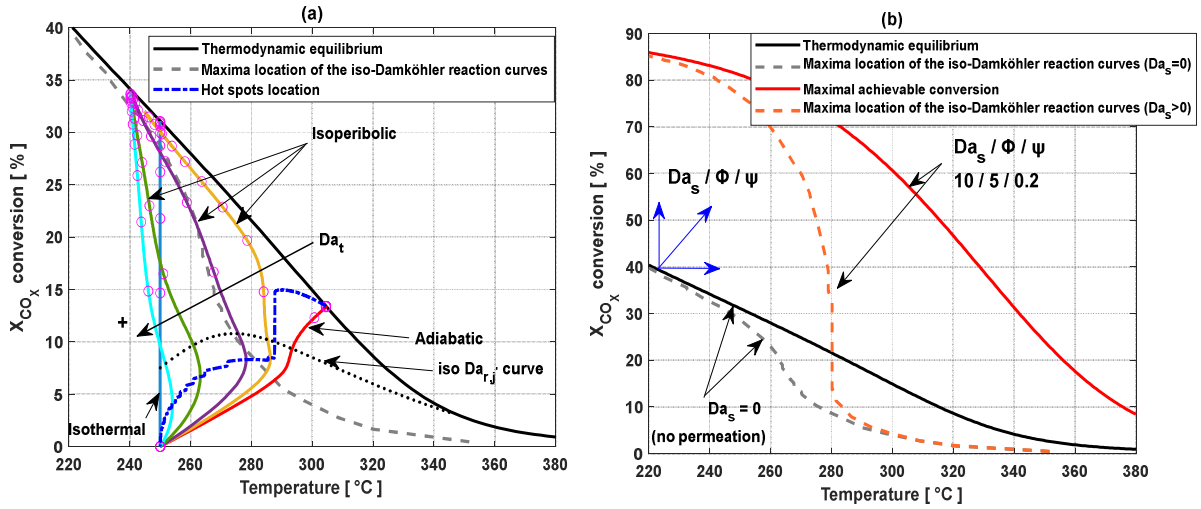

Fig. 4. Impact of coupling to elementary functions, (a) coupling to a heat exchange at $Da_{r,j'} = 25$, $T_f = 240$ °C (b) coupling to membrane separation.

In **Fig. 4**a, the axial evolutions are presented in the plane (Temperature; Conversion) under different exchange modes managed by different values of the characteristic heat-transfer time at a constant heat-transfer fluid temperature ($T_f = 240\,°C$) along the reactor length. The

reactor inlet is observed at coordinates (250 °C;0). The evolution within the reactor is monitored thanks to cyclic markers: the distance between successive circles along the trajectories accounts for a tenth of the reactor length. The black curve represents the thermodynamic equilibrium at P_{in}^{RZ} = 5 MPa. The vertical straight line shows the evolution within an isothermal reactor. The continuous curves depict the evolution within the reactor at different heat-exchange rates with the coolant. Due the exothermic process nature, when the characteristic heat-transfer time is greater than the characteristic reaction time, a hot spot appears at the reactor inlet: the dashed blue curve defines the location of the hot spot maxima at different heat-exchange rates in this (T; X) plane. This curve can be shifted in the plane (Temperature; Conversion) by modifying the inlet temperature. The grey dashed curve represents the maxima location of the iso-$Da_{r,j'}$ curves: this curve is the interface between the kinetic and thermodynamic limitation regimes. One can observe that the iso-$Da_{r,j'}$ curve (black dotted curve) reaches a maximum by increasing the heat-transfer time, which then drops again and approaches the thermodynamic equilibrium. However, it should be mentioned that coupling to a heat exchanger allows, for these reactions, to follow this trajectory of maxima and to minimize the necessary reactor volume by maximizing the reaction rate at any point, thus, allowing the design of more compact equipment adapted to delocalized production. **Fig. 4**a also confirms what was mentioned above regarding **Fig. 3**d: the faster the heat exchange, the more the initial slope of the curve in isoperibolic mode deviates from that of the adiabatic mode ($Da_t = 0$) at the reactor inlet.

In **Fig. 4**b, coupling to separation membrane increases the maximum achievable conversion at a given temperature. The maximum achievable conversion depends both on the three dimensionless numbers (Da_s, ψ and Φ). The evolution direction is indicated on the plane (Temperature; Conversion) by the blue arrows according to the considered parameter values.

In the following, cartographic representations will be used to define global ranges of transfer phenomena rates in order to identify the various limiting mechanisms, and to show how the coupling between these elementary functions would be beneficial for both of them.

3.1 Reaction-Separation coupling

Fig. 5 shows the effect of $Da_{r,j'}$ and Da_s on the final CO_X (CO_2+CO) conversion for ideal water permselectivity $\left(S_{H_2O/H_2} = \infty\right)$ (**Fig. 5**a) and real permselectivity $\left(S_{H_2O/H_2} = 38\right)$ (**Fig. 5**b) at T_{in} = 250 °C (isothermal mode).

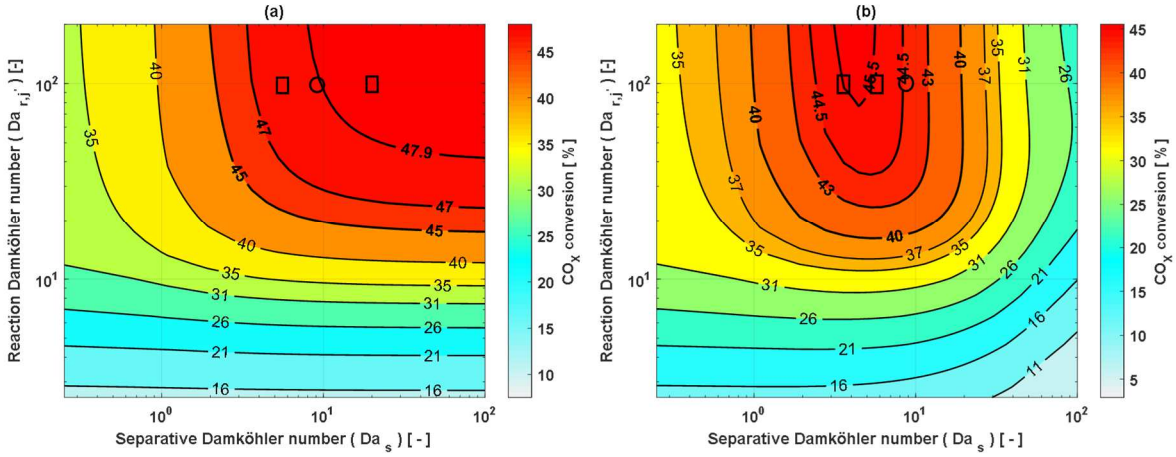

Fig. 5. Effect of reaction Damköhler number and separative Damköhler number on CO_X conversion for various membrane permselectivities with respect to H_2O and H_2, (a) $S_{H_2O/H_2} = \infty$ (b) $S_{H_2O/H_2} = 38$. (ψ = 0.8 and Φ = 1); ○ profiles presented in **Fig. 6**; □ profiles presented in **Fig. 7**.

In **Fig. 5**a, it should be mentioned that, in the case of a large reaction time (slow reaction), the rate of the overall process depends only on the reaction rates. This means that in the low $Da_{r,j'}$ region, the process is limited by reaction kinetics and the coupling to a membrane is not useful. For a very large or very small characteristic transfer time through the membrane (very small Da_s (data not shown in **Fig. 5**a) or very large Da_s, respectively), a conversion plateau appears and shows almost no sensitivity to $Da_{r,j'}$ and/or Da_s. This can be explained

as follows: in the low Da_s region, the characteristic transfer time through the membrane is much larger than the reaction time: the transfer through the membrane is unable to remove water properly leading to an equilibrium plateau. Under these conditions, the process is limited by the transfer through the membrane. At high $Da_{r,j'}$ values, membrane permeation enables to remove water from the reaction zone, but, at same time, enriches the permeation zone rapidly with the permeated species. This decreases the driving force along the reactor length, reducing the usefulness of the membrane coupling only to the upstream of the reactor as shown in **Fig. 6**. In region with high $Da_{r,j'}$, the conversion is very sensitive to the permeation rate through the membrane in the Da_s range between 0.6 and 10.

Fig. 5 shows not only the ranges of reaction and separative Damköhler numbers to be considered to reach a specific conversion, but also that the optimum point is shifted to the left if the membrane is not ideally water-selective (**Fig. 5**b). The zone in which a plateau with a relatively high reaction Damköhler is observed in **Fig. 5**a does not exist in the case of a non-ideal membrane ($S_{H_2O/H_2} \neq \infty$): the conversion is much more sensitive to the permeation rate through the membrane. In this case, the characteristic reaction time and the transfer time through the membrane are comparable. This being said, there is an optimal balance between the two phenomena at a given permselectivity. The shift of the optimum to the left from ideal case is justified as follows: the reduction of the transfer time through the membrane accelerates the species permeation through the membrane. However, a very high permeation rate also accelerates the hydrogen loss from the reaction zone, forcing the equilibrium to move in the opposite direction. Consequently, considering the membrane permselectivity is necessary for proper design optimization.

In order to get a parallel view of what is happening within the reactor, **Fig. 6**a and **Fig. 6**b present the water and hydrogen partial pressures evolution within the membrane reactor for

different selectivities in the two zones and within the conventional reactor (CR) at $Da_{r,j'}$ = 100 and $Da_s = 8$. Similarly, **Fig. 6**c and **Fig. 6**d show the evolution of the corresponding dimensionless molar flow rate profiles.

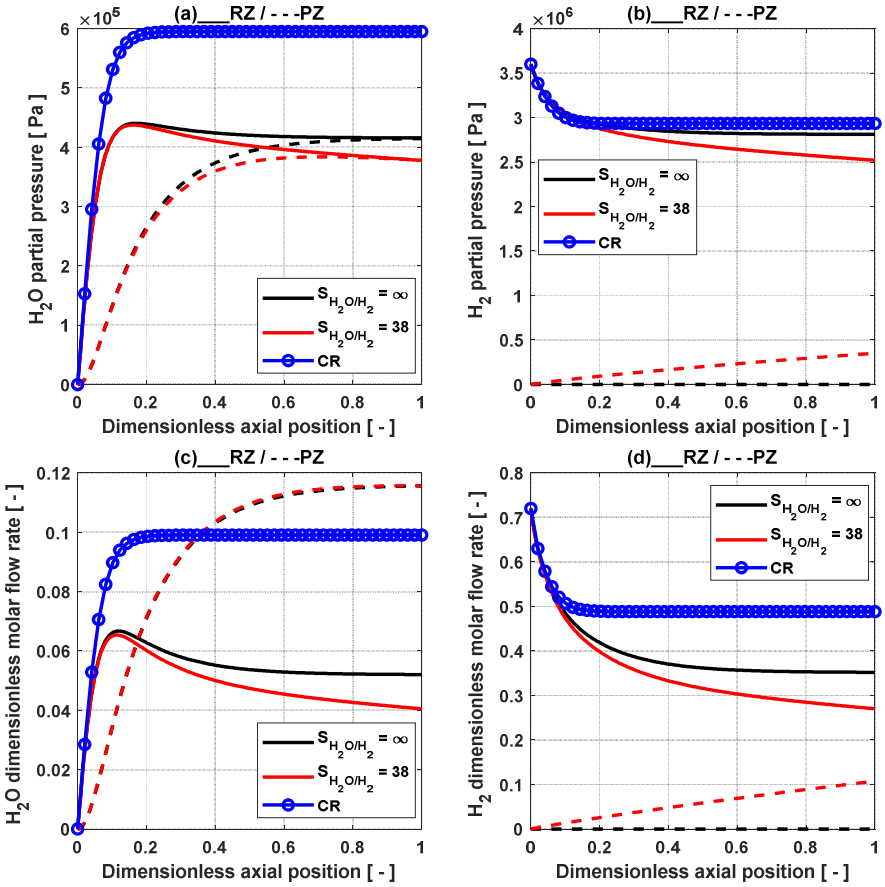

Fig. 6. Evolution of the water and hydrogen partial pressure profiles along the membrane reactor (in the reaction (RZ) and permeation (PZ) zones) and a conventional reactor (CR). ($Da_{r,j'}$ = 100, Da_s = 8, ψ = 0.8 and Φ = 1, isothermal mode);

These representations confirm the comments described above and show the drop in driving force along the reactor. **Fig. 6** shows that the water profile presents a maximum in the vicinity of the reactor inlet, and also merges with the profile encountered in a conventional reactor. This is explained by a water production time (reaction time) lower than the time of its permeation through the membrane: in this zone, the process is limited by the transfer through

the membrane. It should be mentioned that coupling to membrane is not only limited by the permeation rate but also to the correct parameterization of other factors influencing the membrane reactor performance.

Fig. 7 presents an overview of the species evolution within the reactor for two different points extracted from the cartographic presentation discussed in **Fig. 5** at $Da_{r,j'} = 100$. **Fig. 7**a and **Fig. 7**b illustrate the dimensionless profiles evolution for $S_{H_2O/H_2} = \infty$ at different permeation rates.

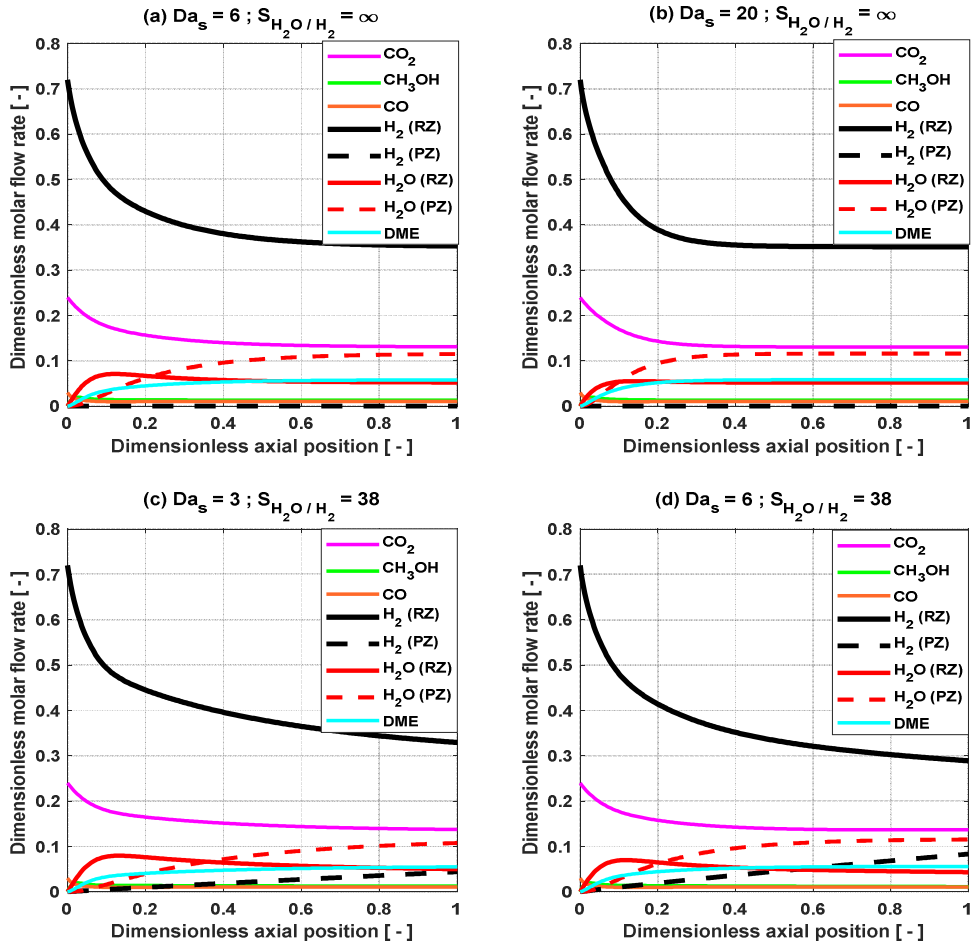

Fig. 7. Evolution of the dimensionless molar flow rate of species along the membrane reactor, (a) Da_s= 6, $S_{H_2O/H_2} = \infty$, (b) Da_s= 20, $S_{H_2O/H_2} = \infty$, (c) Da_s= 3, $S_{H_2O/H_2} = 38$, (d) Da_s= 6, $S_{H_2O/H_2} = 38$. ($Da_{r,j'} = 100$, isothermal mode);

Even if the final conversions obtained at the reactor outlet are very close, the evolutions within the reactor are slightly different. In the case of a low characteristic transfer time through membrane (**Fig. 7**b), the water is quickly transferred from the reaction zone and an equilibrium is established before the reactor half. At the same time, the permeation zone is quickly enriched with the permeated species. For a lower membrane transfer rate (**Fig. 7**a), the evolution within the reactor is slower and equilibrium is almost reached at the rector outlet: the limitations by transfer through the membrane are more significant compared to case (b).

Fig. 7c and **Fig. 7**d show the evolution of dimensionless profiles for $S_{H_2O/H_2} = 38$ at different permeation rates. Although a lower transfer time through the membrane (**Fig. 7**d) removes water rapidly from the reaction zone compared to a relatively large time (**Fig. 7**c), that induces a higher loss of hydrogen from the reaction zone. Given the significance of hydrogen in this type of process, the hydrogen should be recovered by the sweep gas recycling and further water condensation, which could serve to feed the electrolyzer again.

3.1.1 Effect of pressure and sweep flow rate ratios (ψ and Φ)

Fig. 8 and **Fig. 9** present the effect of $Da_{r,j'}$ and Da_s on the CO_X final conversion at different sweep flow rate ratios (Φ) and pressure ratios (ψ) for $S_{H_2O/H_2} = \infty$ and $S_{H_2O/H_2} = 38$, respectively. For the different ψ considered, the pressure in the reaction zone is set at 5 MPa. Figures on the left (a, b and c) show the results obtained for Φ =1, 5 and 10 respectively, at ψ = 0.8. Figures on the right side (d, e and f) show the results obtained for Φ =1, 5 and 10 respectively, at ψ = 0.2.

The simulation results show that a low ψ is always helpful for performance improvement at any Φ. This is mainly related to higher transmembrane flow thanks to a higher driving force. A figure will be presented later to describe this effect. In the same context, at a fixed pressure

ratio, the increase in the sweep flow rate ratio is also beneficial. A high appropriate sweep gas flow rate keeps the water partial pressure in the permeation zone as low as possible, avoiding the rapid enrichment of the permeation zone by the permeated species and enabling more permeation for an identical characteristic transfer time through the membrane. Therefore, the transmembrane flux through the membrane is higher.

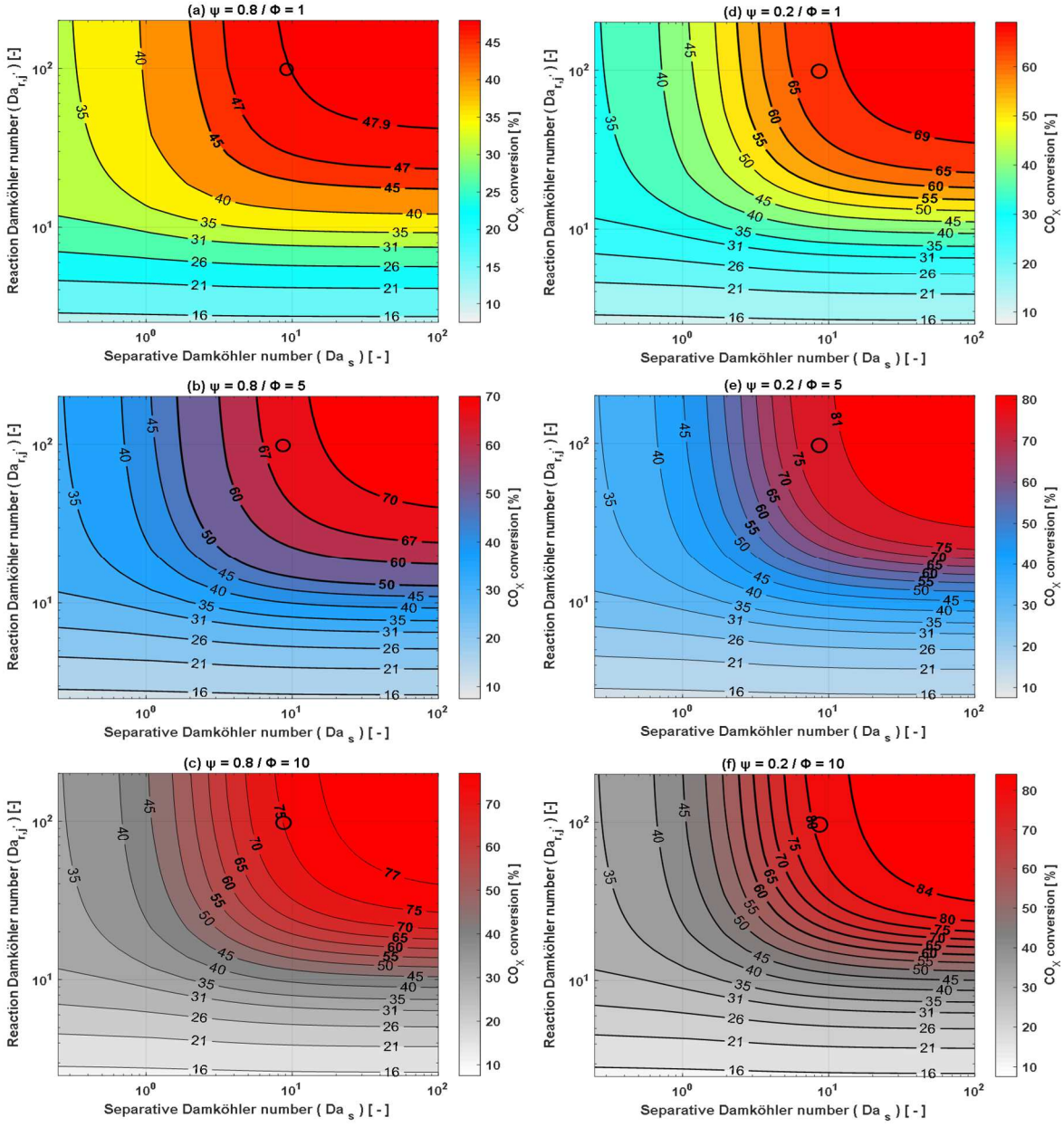

Fig. 8. Effect of reaction Damköhler number and separative Damköhler number on CO_X conversion for various sweep flow rate (Φ) and pressure (ψ) ratios at $S_{H_2O/H_2} = \infty$ and $P_{in}^{RZ} =$

○

5 MPa, (a) ψ = 0.8, Φ = 1 (b) ψ = 0.8, Φ = 5 (c) ψ = 0.8, Φ = 10 (d) ψ = 0.2, Φ = 1 (e) ψ = 0.2, Φ = 5 (f) ψ = 0.2, Φ = 10; profiles presented in **Fig. 10**.

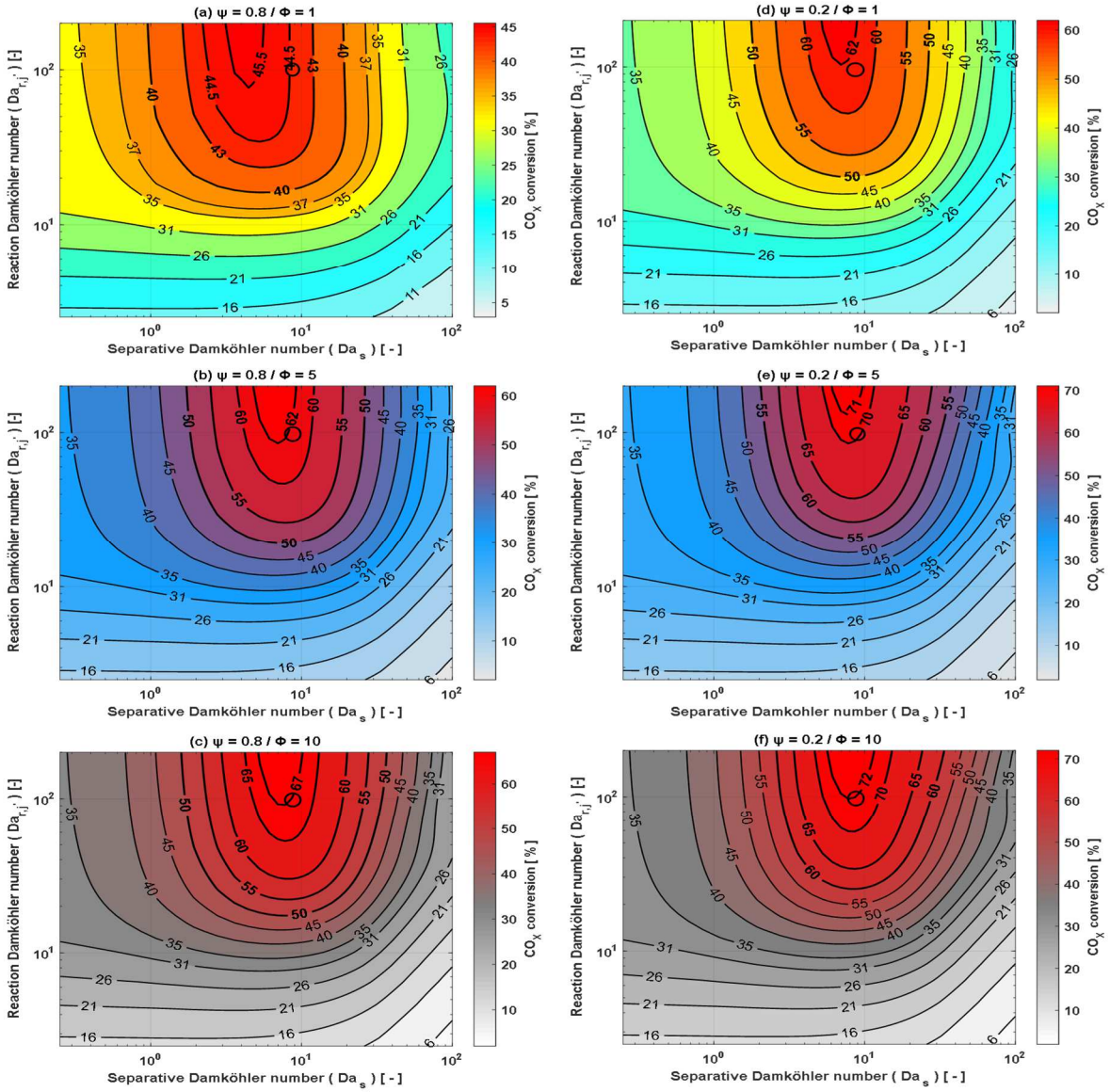

Fig. 9. Effect of reaction Damköhler number and separative Damköhler number on CO_X conversion for various sweep flow rate (Φ) and pressure (ψ) ratios at S_{H_2O/H_2} = 38 and P_{in}^{RZ} = 5 MPa, (a) ψ = 0.8, Φ = 1 (b) ψ = 0.8, Φ = 5 (c) ψ = 0.8, Φ = 10 (d) ψ = 0.2, Φ = 1 (e) ψ = 0.2, Φ = 5 (f) ψ = 0.2, Φ = 10; profiles presented in **Fig. 10**.

These two parameters (ψ and Φ) have a positive effect on the membrane reactor performance: limitation by transfer through the membrane can be reduced. By contrast, it is

necessary to choose a trade-off between these two factors in order to maintain a high transmembrane driving force without consuming excessive energy. Energetically, it is interesting to mention that low ψ values penalize less the process as soon as vacuum is not used in the sweep. For example, $P_{in}^{RZ} = 5\,MPa$ and $\psi = 0.02$ could indicate atmospheric pressure in sweep side. It is worth mentioning that the same trends are obtained for each of CO_2 conversion, DME yield and DME selectivity with ranges from 45.5 to 85 %, 43.2 to 83.5 % and 90 to 98.3 %, respectively, at the reactor outlet.

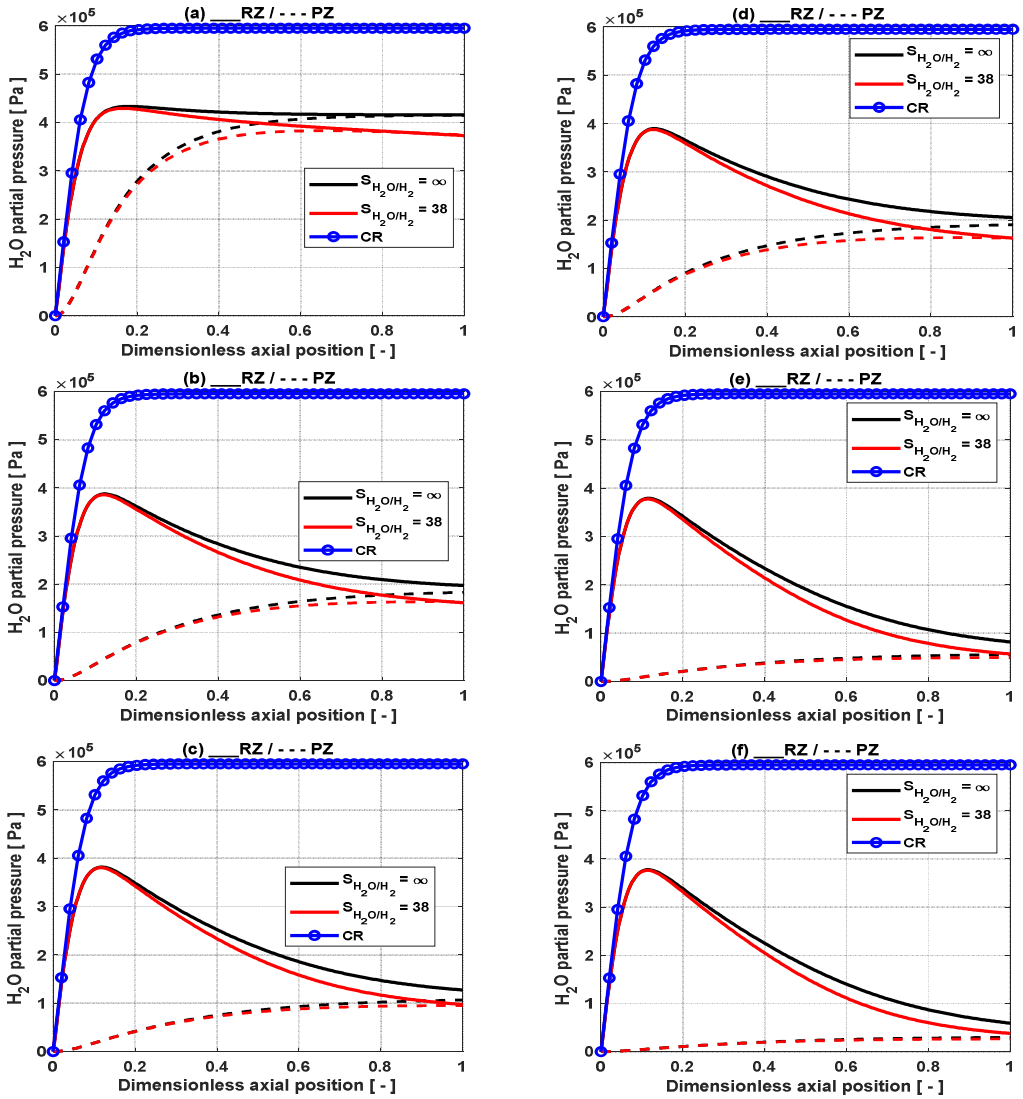

Fig. 10. Evolution of the water partial pressure profile along the membrane reactor (in the reaction (RZ) and permeation (PZ) zones) and a conventional reactor (CR) at $Da_{r,j'} = 100$

and Da_s = 9, (a) ψ = 0.8, Φ = 1, (b) ψ = 0.8, Φ = 5, (c) ψ = 0.8, Φ = 10, (d) ψ = 0.2, Φ = 1, (e) ψ = 0.2, Φ = 5, (f) ψ = 0.2, Φ = 10.

Fig. 10 describes the effect of these parameters (ψ and Φ) on the driving force for a given point, marked by a circle in **Fig. 8** and **Fig. 9** while keeping the same order of presentation.

These figures confirm that the increase in Φ and the decrease in ψ in this case ensure a significant driving force able to reduce the limitations by transfer through the membrane. **Fig. 10** also shows that from a certain couple (ψ, Φ) the maximum of the water partial profile near the reactor inlet is no more influenced by these parameters: the process remains limited in these conditions by the transfer through the membrane.

Fig. 11 shows the way to adapt the transfer time through the membrane according to the permselectivity S_{H_2O/H_2}, and conversely, in order to reach a given CO_X conversion.

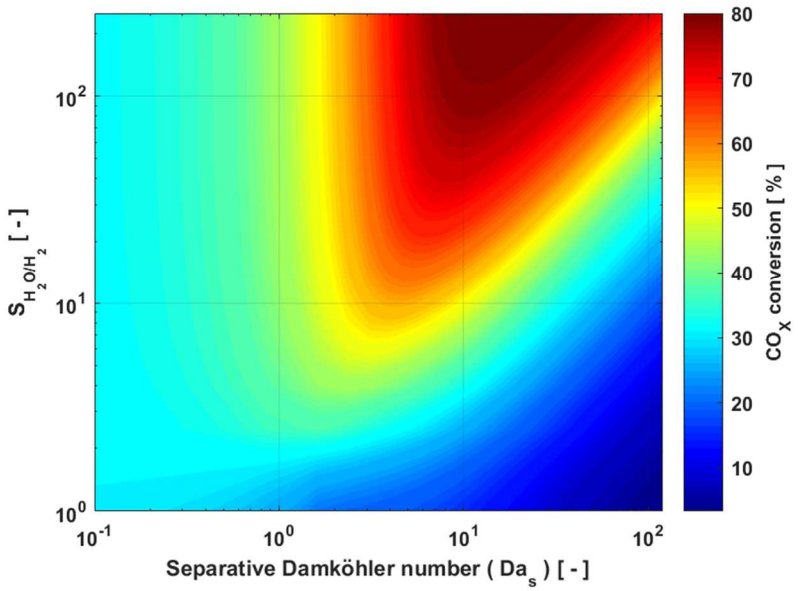

Fig. 11. Effect of membrane permselectivity (S_{H_2O/H_2}) and separative Damköhler number on CO_X conversion at $Da_{r,j'}$= 100.

For a large transfer time through the membrane (low Da_s), the effect of permselectivity is not significant because the membrane reactor behavior is close to a conventional reactor. For

membranes with low permselectivities, short transfer times through the membrane (high permeation rates) are not suitable for process improvement due to the reagents loss through the membrane. Coupling to this membrane type is not recommended. It is worth mentioning that the optimum location on this map is always the same regardless of ψ and Φ: only the optimum value changes according to ψ and Φ as shown above. In general, developing membranes with high permselectivities that do not ensure a proper permeation rate, or developing membranes with high permeation rates but low permselectivities, is not useful for this type of process: a trade-off between the transfer time through the membrane and permselectivity is beneficial. It should be mentioned that a minimum permselectivity of 30 is required to access a configuration where membrane coupling offers significant improvements compared to conventional reactors: this gain is attainable for a Da_s larger than 4 according to the membrane permselectivity considered.

This permselectivity condition is satisfied for current zeolite membranes[51]. The next section discusses how coupling to heat exchange could be beneficial in such a configuration, providing a win-win coupling between these elementary functions.

3.2 Reaction-Exchange / Reaction-Exchange-Separation couplings

The exothermic nature of this kind of process induces the presence of hot spots at the reactor inlet. This hot spot generally appears in this zone because of a significant transformation driving force due to the high concentrations of reagents in this zone. This means that the characteristic heat-transfer time is larger than the characteristic reaction time: the process is limited in these regions by the heat transfer. **Fig. 4**a had previously shown the existence of hot spots at different Da_t. The hot spot intensity decreases with the decrease in the characteristic heat-transfer time (increasing Da_t).

The first part of this work showed that current membranes can provide a considerable improvement over conventional reactor if they are not exposed to high temperature conditions. In addition, **Fig. 10** also showed that the membrane relevance is more pronounced upstream of the reactor due to a significant driving force, and **Fig. 11** showed that coupling to a membrane with low permselectivity reduces its relevance. One of the main factors reducing the membrane permselectivity is the high temperature. However, according to all these considerations, in order to preserve the properties of the currently available membranes, and to maintain the catalyst activity, coupling with an efficient heat exchange is a priority before integrating the currently available membranes.

Before discussing the coupling between the three elementary functions, an optimization of both the catalyst mass and the hot spot intensity within the reactor is presented. This point consists in the catalyst dilution in some zones of the reactor with inert solid as defined in **Table 6**. The inert solid density is considered the same as that of the bifunctional DME synthesis catalyst. This is managed on MATLAB by a reactor discretization with the addition of a parameter θ ($0 \leq \theta \leq 1$) in the first term of the mass and heat balance equations. Where θ is given by $\theta = m_{cat}/(m_{cat} + m_{inert,s})$. The catalyst distribution in **Table 6** is proposed after dealing with this case separately from this paper.

Table 6
Catalyst distribution within the reactor.

Dimensionless axial location (-)	Active catalyst (%)	Inert solid (%)
0-0.15	40	60
0.15-0.25	55	45
0.25-0.5	80	20
0.5-0.75	90	10
0.75-1	100	0

Fig. 12 shows both the effect of $Da_{r,j'}$ and Da_t on CO_X conversion at the reactor outlet and on the hot spot reached within the reactor for two different configurations of catalyst distribution within the reactor. **Fig. 12**a and **Fig. 12**c correspond to a conventional case of catalyst distribution along the reactor (0% inert). **Fig. 12**b and **Fig. 12**d correspond to the proposed catalyst distribution (**Table 6**).

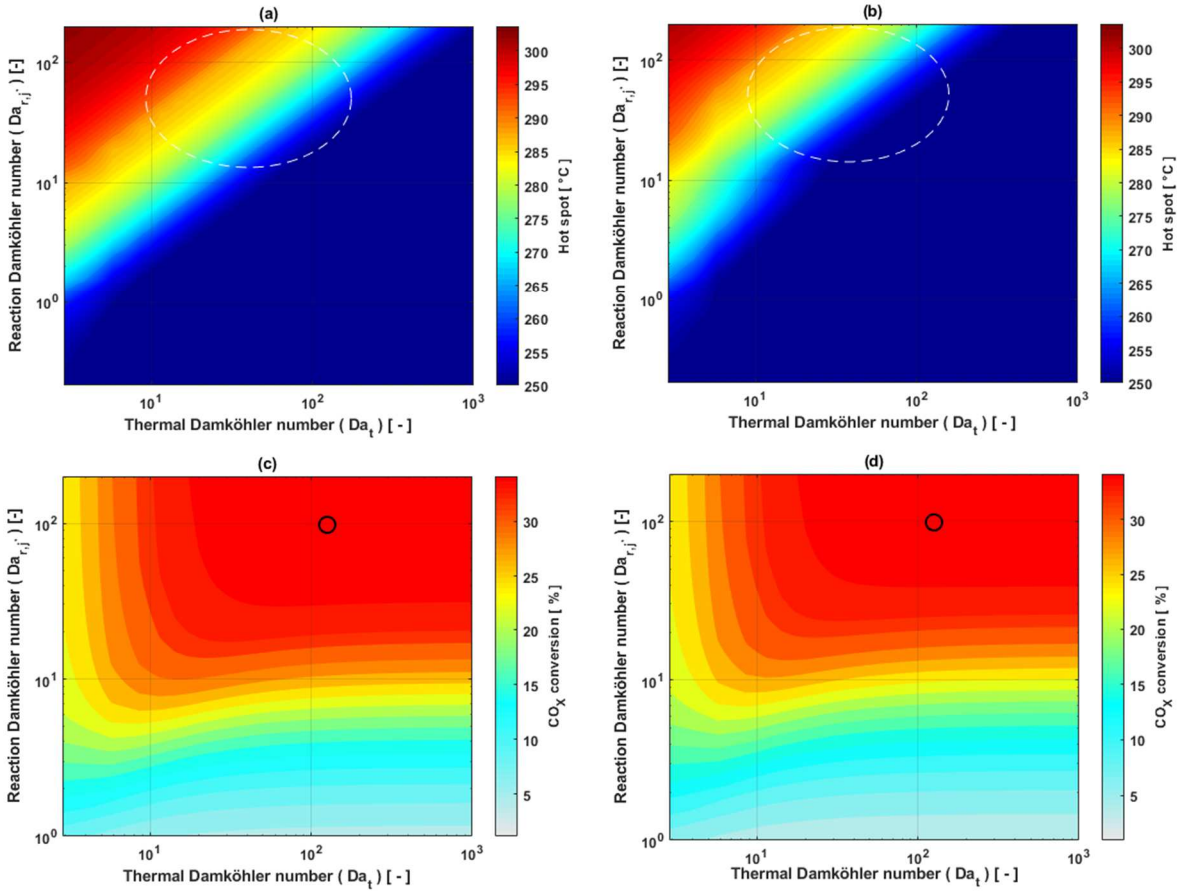

Fig. 12. Effect of reaction Damköhler number and thermal Damköhler number on CO_X conversion for different catalyst distributions within the reactor, (a, c) conventional uniform catalyst distribution, (b, d) catalyst dilution in some reactor zones according to **Table 6**; T_f = 240 °C, ○ profiles presented in **Fig. 13**.

In low $Da_{r,j'}$ regions, the process is always limited by reaction kinetics. For a relatively high $Da_{r,j'}$, the process is even more limited by heat transfer the higher its characteristic time.

For a $Da_t = 0$, the reactor operates in adiabatic mode and the conversion is always lower than that in the case with heat transfer through the reactor wall (thermodynamic equilibrium limitation).

Fig. 12 shows that the less efficient the heat exchange (sense of Da_t decrease) the higher the hot spot within the reactor. Moreover, from a certain heat-transfer time, no conversion progress is observed due the equilibrium conditions. However, it should be mentioned that there exists an optimal characteristic heat-transfer time at which conversion is maximized while keeping a low hot spot within the reactor without reactor oversizing.

The new catalyst distribution proposed makes it possible to reduce the intensity of the hot spot at the reactor inlet for an identical outlet conversion in the interesting $Da_{r,j'}$ regions. This configuration allows to reduce the very low characteristic heat-transfer time requirement compared to the conventional case in order to meet the objective of a maximum conversion and a minimum hot spot. This can be observed in **Fig. 12** (dashed ellipses) by milder areas at a given Da_t for an identical outlet conversion. This catalyst distribution allows not only to meet this objective but also to meet an economic criterion, since an economic gain is obtained by the use of a lower active catalyst mass for an identical output conversion (21% total catalyst reduction).

Fig. 13a presents an overview of a configuration extracted from cartographic representations shown in **Fig. 12**. **Fig. 13**b shows the corresponding water partial pressure profiles along the reactor for the two catalyst distributions ((1): uniform catalyst distribution, and (2): catalyst distribution according to **Table 6**) with an identical heat-transfer time.

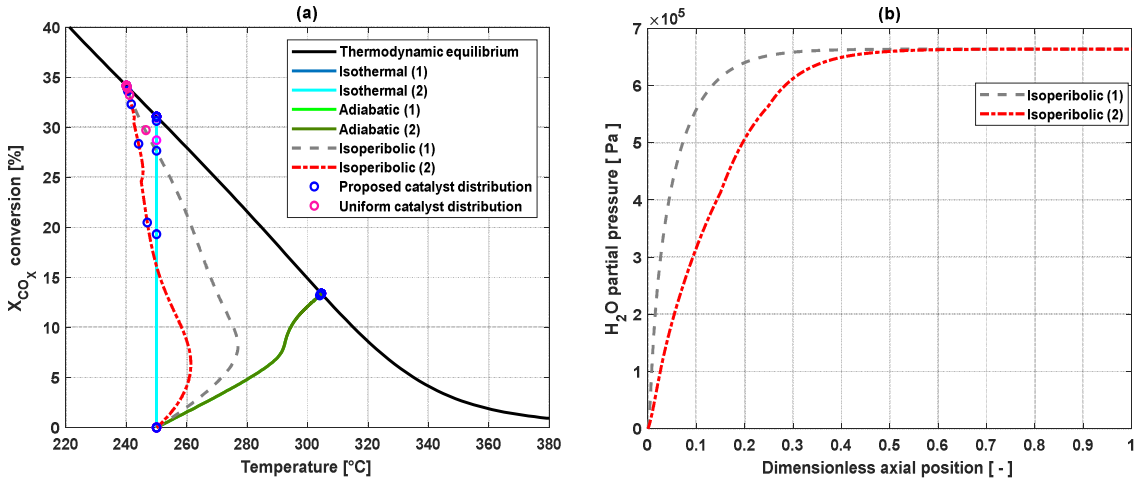

Fig. 13. Effect of the different catalyst distributions on the evolution within the reactor, (a) impact on conversion and temperature (b) impact on the water production rate.

Fig. 13a shows different behaviors within the reactor for the different catalyst distributions (except for the adiabatic mode), but the final conversion is identical. For the same characteristic heat-transfer time, the proposed catalyst distribution configuration (case: isoperibolic (2)) reduces the hot spot intensity by around 18 °C compared to the uniform catalyst distribution configuration (case: isoperibolic (1)). **Fig. 13**b shows that the water production rate is reduced at the reactor inlet compared to the conventional case (isoperibolic (1)). This result allows a relatively high reaction time in this zone, which the subsequent coupling to a membrane can benefit from: the limitations by transfer through the membrane could be reduced. As a result, a proper catalyst distribution within the reactor and an efficient heat transfer allow both to preserve the catalyst metallic function and to make the membrane coupling more beneficial. This approach also allows to reproduce the isothermal simulations results of the first section.

The new catalyst distribution configuration will be taken into account for the next results. In order to have a broad insight regarding the coupling of these elementary functions, the effect of the characteristic time ratios is displayed in **Fig. 14** at different targeted conversion level

($Da_{r,j'}$ = 20 and 80), and for different membrane permselectivities ($S_{H_2O/H_2} = \infty$ and $\neq \infty$). The values of the permselectivity (S_{H_2O/H_2}) as a function of temperature are computed thanks to a fitting on MATLAB (Trust-Region algorithm, Bisquare method and 95% confidence bounds) of the experimental points presented in the work of Rohde et al. [51] in a temperature range from 200 to 350 °C, based on an Arrhenius-type law (equation (14)):

$$S_{H_2O/H_2} = 9.508 * 10^{-3}\, exp(3.605 * 10^4/R/T) \quad (14)$$

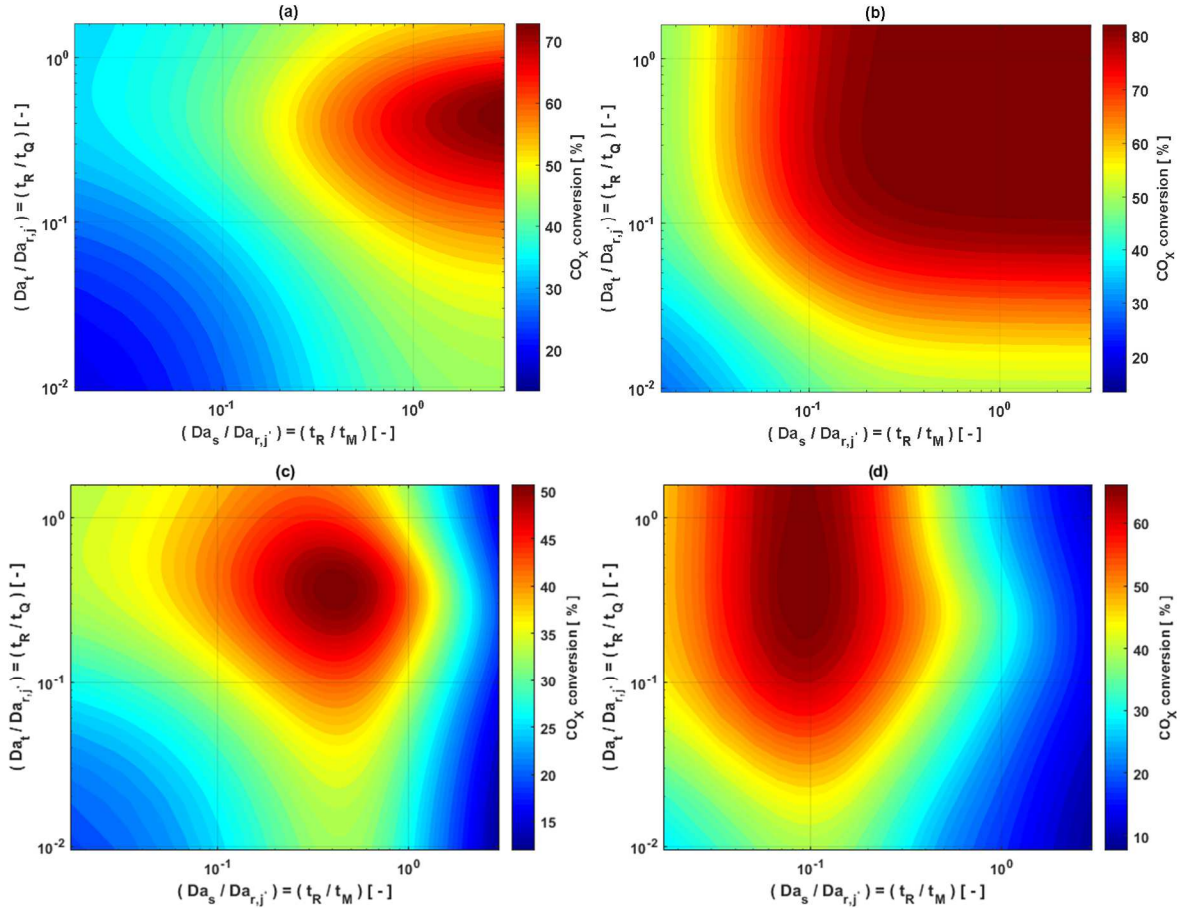

Fig. 14. Effect of characteristic time ratios on process improvement, (a) $S_{H_2O/H_2} = \infty$, $Da_{r,j'}$= 20 (b) $S_{H_2O/H_2} = \infty$, $Da_{r,j'}$ = 80 (c) $S_{H_2O/H_2} \neq \infty$, $Da_{r,j'}$ = 20 (d) $S_{H_2O/H_2} \neq \infty$, $Da_{r,j'}$ = 80, ψ = 0.2, Φ = 5.

The analysis of these maps provides an overview of the rates characterizing each phenomenon. In order to understand the physical meaning, when the characteristic heat-

transfer time is lower than the reaction time, the heat transfer is able to efficiently remove the heat generated by reactions. Similarly, when the characteristic transfer time through the membrane is lower than the reaction time, the membrane transfer can effectively remove the target species from the reaction zone. In these two cases, the overall process rate depends only on the reaction rates: the process is limited by reaction kinetics. Otherwise, when the characteristic heat-transfer time is larger than the reaction time, the heat transfer cannot remove the generated heat in the reaction zone as fast as it appears. In this case, the overall process rate is limited by heat-transfer rate. Likewise, when the characteristic transfer time through the membrane is larger than the reaction time, the membrane is not able to sufficiently remove the targeted species from the reaction zone, and the overall process rate is limited by the transfer through the membrane. However, in the case of coupling between these three elementary functions, the overall process rate could be limited by both heat transfer and transfer through the membrane.

In the previous paragraphs, it has been shown that for low reaction Damköhler ($Da_{r,j'}$) the process is always limited by reaction kinetics. For this reason, relatively high $Da_{r,j'}$ have been chosen in **Fig. 14**. The analysis of these maps allows to understand the phenomenon which should impose its performance with respect to the others.

Fig. 14 indicates the compatibility between reaction, exchange and separation: for a large transfer time through the membrane and a large heat-transfer time, the conversion is very low because the reactor behavior is similar to that of a conventional membraneless reactor in adiabatic mode where conversion is strongly limited by thermodynamic equilibrium. The location of the optimum in **Fig. 14** shows that the membrane selectivity plays an important role in the reactor design optimization. The results clearly reveal the requirement of a trade-off between these couplings in order to achieve optimal conditions. Under the considered

operating conditions, **Fig. 14** shows that a heat-transfer time relatively larger than the reaction time is preferred to reach the optimum area.

In the case of a real permselectivities $\left(S_{H_2O/H_2} \neq \infty\right)$ (**Fig. 14**c), for a medium $Da_{r,j'}$, the requirements in terms of transfer time through the membrane are similar to those for heat-transfer time to achieve optimal results. Both characteristic times, whether for mass transfer through the membrane or heat transfer, remain slightly larger than the reaction time to achieve the best conversion. This is explained, on the one hand, by a heat-transfer time relatively larger than the reaction time for the exploitation of part of the heat generated by the reactions to accelerate the kinetics. On the other hand, a characteristic time through the membrane relatively larger than the reaction time is useful to avoid the hydrogen permeation from the reaction zone to the permeation zone. At a given heat-transfer time, a shorter transfer time through the membrane (high permeation rate) is not advised from a certain permeation rate limit: this is mainly related to the loss of hydrogen through the membrane. This limit shifts towards the high transfer times through the membrane as the desired level of conversion increases as shown in **Fig. 14**d. For this reason, in the case of a high desired conversion (**Fig. 14**d), a heat-transfer time smaller than the transfer time through the membrane becomes necessary to reach the optimal zone. In this context, a lower heat-transfer time than the mass-transfer time through the membrane is recommended to avoid the decrease in permselectivity with temperature that causes the reagent loss. **Fig. 14**c and **Fig. 14**d show that the coupling to membranes with low permselectivities is not useful: a reaction-heat exchange configuration is better. In contrast, **Fig. 14**c and **Fig. 14**d show how the coupling to a heat exchange enables to properly use the membrane and to avoid the problem of decreasing permselectivity with temperature.

In the case of ideal permselectivity ($S_{H_2O/H_2} = \infty$), where hydrogen is kept in the reaction zone, for a medium $Da_{r,j'}$, **Fig. 14**a indicates the need for, at least, equality between reaction time and transfer time through the membrane to achieve optimal conditions. In the case of high $Da_{r,j'}$ (**Fig. 14**b), the results show that an optimal result can be achieved without reactor oversizing. For a given heat-transfer time, the displacement to the optimal zone can be ensured by improving the transfer through the membrane to a certain level. The same observation holds for a given transfer time through the membrane. This point reflects the sacrifice of one to the other in order to improve the reactor performance. It has to be mentioned that the same trends are obtained for DME selectivity and CO_2 conversion. Selectivity and conversion are improved due to the water removal where methanol dehydration is not inhibited, and reactants partial pressures are not affected by dilution. In addition, due to the heat removal, catalyst deactivation is avoided, and the process temperature is brought into areas where the reaction rate is not inhibited by thermodynamic limitation.

The knowledge of these ratios clearly shows how the geometrical dimensions influence the rate of the different phenomena as shown in **Table 4** and by equations (15) and (16), where t_R denotes the characteristic reaction time, t_M is the characteristic transfer time through the membrane, t_Q is the characteristic heat-transfer time, m_{cat} is the catalyst mass, Ă is the total active membrane area, a is the interfacial area of heat transfer per unit reactor volume (V_{reac}), $\mathcal{P}_{H_2O}$ is the water permeance and U is the overall heat-transfer coefficient.

$$\frac{\check{A}}{m_{cat}} = \frac{t_R}{t_M}\frac{k_j}{\mathcal{P}_{H_2O}}\frac{P^{\delta_j}}{P^{RZ}} \tag{15}$$

$$\frac{a}{m_{cat}} = \frac{t_R}{t_Q}\frac{k_j}{U\,V_{reac}} P^{\delta_j}\,\widetilde{FCp} \tag{16}$$

The definition of these characteristic time ratios also allows to identify the operating parameters set by the process operating conditions (GHSV, etc.). However, a good understanding of these characteristic times leads to the definition of a good approach for the intensified reactor design while suppressing, as much as possible, all limitations that reduce reactor performances. A subsequent process optimization study should be established on the basis of these principles.

4. Conclusions

This paper has presented a physically-comprehensible approach based on the application of characteristic time analysis and dimensionless Damköhler numbers to a process intensification problem related to the coupling of three elementary functions: catalytic reaction, heat exchange and membrane separation. The application of this analysis contributes to process innovation and is essential for proposing most relevant intensification strategies. Coupling between reaction, heat exchange and membrane separation demonstrated the synergy between these functions leading to the identification of the optimal operating conditions and configuration.

The results of this approach show that coupling to a membrane improves the performance of conventional reactors over a certain conversion range. To make membrane coupling beneficial, a good parameterization of additional factors (ψ, Φ, etc.) influencing the membrane reactor performance is required. A trade-off between these factors enables to maintain a high transmembrane driving force without consuming excessive energy to maintain a significant pressure difference between the two zones. The membrane reactor performance is not only influenced by these factors, but also by a heat-exchange coupling. Results show how efficient heat exchange allows for proper membrane operation, and how coupling to the membrane allows for an improved configuration of a heat-exchange reactor.

Simulation results have shown that, despite the minimized loss of hydrogen thanks to a good heat exchange that avoids the decrease of permselectivity with temperature, the membrane reactor performance remains better than a conventional reactor. This membrane type exhibiting high permselectivities for H_2O and H_2 is already reported in the literature. They generally have to face to stability issues at high temperatures. A good heat exchange makes this type of membranes promising. For the CO_2 permeation, an efficient heat exchange and proper operating conditions will also significantly minimize CO_2 permeation, and its consideration in this case will not affect the results obtained. Alternatively, conventional zeolite membranes also allow the methanol permeation through the membrane. To avoid the problem of species permeation, literature works propose the presence of the same species in both reaction and permeation zones to minimize the driving force of mass-transfer through the membrane, either by identical sweep feed or by recycling of the sweep gas. Due to economic costs and technical feasibility, the development of membranes allowing, at most, the permeation of small molecules remains preferred.

The present work revealed that the proposed catalyst distribution in the reactor allows to reach similar results at the reactor outlet as the uniform catalyst distribution. This distribution allows a 21% reduction of the total mass of active catalyst, and a significant reduction in the hot spot intensity within the reactor. This distribution slows down the water production rate at the reactor inlet. This observation challenges what is often reported in the literature that coupling to a membrane in co-current mode is always better than the counter-current mode due to the high water concentration at the reactor inlet. With slower water production rate at the reactor inlet, the counter-current mode could be treated as a perspective and compared to the co-current mode.

The applied approach can be flexibly extended for other balanced exothermic reactions. In order to further improve this approach and to propose new methodological structures, optimization methods could be used additionally in the subsequent works in order to provide the parametric optimization of the process to be intensified.

Declaration of Competing Interest

The authors declare that they have no known competing financial interests or personal relationships that could have appeared to influence the work reported in this paper.

Acknowledgments

The authors would like to thank the French MESRI for the funding of the PhD doctoral thesis which supports this research.

References

[1] International Energy Outlook 2020. https://www.eia.gov/outlooks/ieo/ (accessed 16 February 2021).

[2] Catizzone, E.; Bonura, G.; Migliori, M.; Frusteri, F.; Giordano, G. CO_2 Recycling to Dimethyl Ether: State-of-the-Art and Perspectives, Molecules 23 (1) (2017) 31.

[3] Centi, G.; Perathoner, S. Opportunities and Prospects in the Chemical Recycling of Carbon Dioxide to Fuels, Catal. Today 148 (3–4) (2009) 191–205.

[4] Pontzen, F.; Liebner, W.; Gronemann, V.; Rothaemel, M.; Ahlers, B. CO_2-Based Methanol and DME – Efficient Technologies for Industrial Scale Production, Catal. Today 171 (1) (2011) 242–250.

[5] Rubin, E. S.; Davison, J. E.; Herzog, H. J. The Cost of CO_2 Capture and Storage, Int. J. Greenhouse Gas Cont. 40 (2015) 378–400.

[6] Li, B.; Duan, Y.; Luebke, D.; Morreale, B. Advances in CO_2 Capture Technology: A Patent Review, Appl. Energy 102 (2013) 1439–1447.

[7] Yu, C.-H.; Huang, C.-H.; Tan, C.-S. A Review of CO_2 Capture by Absorption and Adsorption, Aerosol Air Qual. Res. 12 (5) (2012) 745–769.

[8] Saeidi, S.; Amin, N. A. S.; Rahimpour, M. R. Hydrogenation of CO_2 to Value-Added Products-A Review and Potential Future Developments, J. CO_2 Util. 5 (2014) 66–81.

[9] Song, C. Global Challenges and Strategies for Control, Conversion and Utilization of CO_2 for Sustainable Development Involving Energy, Catalysis, Adsorption and Chemical Processing, Catal. Today 115 (1) (2006) 2–32.

[10] Leonzio, G.; Zondervan, E.; Foscolo, P. U. Methanol Production by CO_2 Hydrogenation: Analysis and Simulation of Reactor Performance, Int. J. Hydrogen Energy 44 (16) (2019) 7915–7933.

[11] Grové, J.; Greig, C. R.; Smart, S.; Lant, P. A. Producing a CO_2-Neutral Clean Cooking Fuel in India - Where and at What Cost? Int. J. Hydrogen Energy 42 (30) (2017) 19067–19078.

[12] Al-Kalbani, H.; Xuan, J.; García, S.; Wang, H. Comparative Energetic Assessment of Methanol Production from CO_2: Chemical versus Electrochemical Process, Appl. Energy 165 (2016) 1–13.

[13] Atsonios, K.; Panopoulos, K. D.; Kakaras, E. Investigation of Technical and Economic Aspects for Methanol Production through CO_2 Hydrogenation, Int. J. Hydrogen Energy 41 (4) (2016) 2202–2214.

[14] Chen, W.-H.; Lin, B.-J.; Lee, H.-M.; Huang, M.-H. One-Step Synthesis of Dimethyl Ether from the Gas Mixture Containing CO_2 with High Space Velocity, Appl. Energy 98 (2012) 92–101.

[15] Arcoumanis, C.; Bae, C.; Crookes, R.; Kinoshita, E. The Potential of Di-Methyl Ether (DME) as an Alternative Fuel for Compression-Ignition Engines: A Review, Fuel 87 (7) (2008) 1014–1030.

[16] Semelsberger, T. A.; Borup, R. L.; Greene, H. L. Dimethyl Ether (DME) as an Alternative Fuel, J. Power Sources 156 (2) (2006) 497–511.

[17] Alam, M.; Fujita, O.; Ito, K. Performance of NO_X Reduction Catalysts with Simulated Dimethyl Ether Diesel Engine Exhaust Gas. Proceedings of the Institution of Mechanical Engineers, Part A: J. Power and Energy 218 (2) (2004) 89–95.

[18] Kajitani, S.; Chen, Z. Fundamental Research on Next Generation Fuel (Dimethyl Ether) Engines, J. Sci. ind. Res. 62 (01-02) (2003) 133–144.

[19] Song, J.; Huang, Z.; Qiao, X.; Wang, W. Performance of a Controllable Premixed Combustion Engine Fueled with Dimethyl Ether, Energy Conv. Man. 45 (13) (2004) 2223–2232.

[20] Bîldea, C. S.; Győrgy, R.; Brunchi, C. C.; Kiss, A. A. Optimal Design of Intensified Processes for DME Synthesis, Comp. Chem. Eng. 105 (2017) 142–151.

[21] Farsi, M.; Eslamloueyan, R.; Jahanmiri, A. Modeling, Simulation and Control of Dimethyl Ether Synthesis in an Industrial Fixed-Bed Reactor. Chem. Eng. Process.: Process Intensification 50 (1) (2011) 85–94.

[22] Marchionna, M.; Patrini, R.; Sanfilippo, D.; Migliavacca, G. Fundamental Investigations on Di-Methyl Ether (DME) as LPG Substitute or Make-up for Domestic Uses, Fuel Process. Technol. 89 (12) (2008) 1255–1261.

[23] Saravanan, K.; Ham, H.; Tsubaki, N.; Bae, J. W. Recent Progress for Direct Synthesis of Dimethyl Ether from Syngas on the Heterogeneous Bifunctional Hybrid Catalysts, Appl. Catal. B: Environ. 217 (2017) 494–522.

[24] Larson, E. D.; Yang, H. Dimethyl Ether (DME) from Coal as a Household Cooking Fuel in China, Energy for Sustainable Develop. 8 (3) (2004) 115–126.

[25] Semelsberger, T. A.; Ott, K. C.; Borup, R. L.; Greene, H. L. Generating Hydrogen-Rich Fuel-Cell Feeds from Dimethyl Ether (DME) Using Physical Mixtures of a Commercial Cu/Zn/Al2O3 Catalyst and Several Solid–Acid Catalysts, Appl. Catal. B: Environ. 65 (3) (2006) 291–300.

[26] Yoo, J.-H.; Choi, H.-G.; Chung, C.-H.; Cho, S. M. Fuel Cells Using Dimethyl Ether, J. Power Sources 163 (1) (2006) 103–106.

[27] Pérez-Uriarte, P.; Ateka, A.; Aguayo, A. T.; Gayubo, A. G.; Bilbao, J. Kinetic Model for the Reaction of DME to Olefins over a HZSM-5 Zeolite Catalyst, Chem. Eng. J. 302 (2016), 801–810.

[28] Nasser, G.; Kurniawan, T.; Miyake, K.; Galadima, A.; Hirota, Y.; Nishiyama, N.; Muraza, O. Dimethyl Ether to Olefins over Dealuminated Mordenite (MOR) Zeolites Derived from Natural Minerals, J. Nat. Gas. Sci. Eng. 28 (2016) 566–571.

[29] Bauer, M. C.; Kruse, A. The Use of Dimethyl Ether as an Organic Extraction Solvent for Biomass Applications in Future Biorefineries: A User-Oriented Review, Fuel 254 (2019) 115703.

[30] Cordero-Lanzac, T.; Ateka, A.; Pérez-Uriarte, P.; Castaño, P.; Aguayo, A. T.; Bilbao, J. Insight into the Deactivation and Regeneration of HZSM-5 Zeolite Catalysts in the Conversion of Dimethyl Ether to Olefins, Ind. Eng. Chem. Res. 57 (41) (2018) 13689–13702.

[31] Cai, M.; Palčić, A.; Subramanian, V.; Moldovan, S.; Ersen, O.; Valtchev, V.; Ordomsky, V. V.; Khodakov, A. Y. Direct Dimethyl Ether Synthesis from Syngas on Copper–Zeolite Hybrid Catalysts with a Wide Range of Zeolite Particle Sizes, J. Catal. 338 (2016) 227–238.

[32] Spivey, J. J. Review: Dehydration Catalysts for the Methanol/Dimethyl Ether Reaction, Chem.l Eng. Commun. 110 (1) (1991) 123–142.

[33] Azizi, Z.; Rezaeimanesh, M.; Tohidian, T.; Rahimpour, M. R. Dimethyl Ether: A Review of Technologies and Production Challenges, Chem. Eng. Process.: Process Intensification 82 (2014) 150–172.

[34] Mondal, U.; Yadav, G. D. Perspective of Dimethyl Ether as Fuel: Part II- Analysis of Reactor Systems and Industrial Processes, J. CO_2 Util. 32 (2019) 321–338.

[35] Mondal, U.; Yadav, G. D. Perspective of Dimethyl Ether as Fuel: Part I. Catalysis, J. CO_2 Util. 32 (2019) 299–320.

[36] Ereña, J.; Garoña, R.; Arandes, J. M.; Aguayo, A. T.; Bilbao, J. Direct Synthesis of Dimethyl Ether From (H_2+CO) and (H_2+CO_2) Feeds. Effect of Feed Composition, Int. J. Chem. React. Eng. 3 (1) (2005) A44.

[37] Jia, G.; Tan, Y.; Han, Y. A Comparative Study on the Thermodynamics of Dimethyl Ether Synthesis from CO Hydrogenation and CO_2 Hydrogenation, Ind. Eng. Chem. Res. 45 (3) (2006) 1152–1159.

[38] Ng, K. L.; Chadwick, D.; Toseland, B. A. Kinetics and Modelling of Dimethyl Ether Synthesis from Synthesis Gas, Chem. Eng. Sci. 54 (15–16) (1999) 3587–3592.

[39] Iliuta, I.; Iliuta, M. C.; Larachi, F. Sorption-Enhanced Dimethyl Ether Synthesis-Multiscale Reactor Modeling, Chem. Eng. Sci. 66 (10) (2011) 2241–2251.

[40] Iliuta, I.; Larachi, F.; Fongarland, P. Dimethyl Ether Synthesis with in Situ H_2O Removal in Fixed-Bed Membrane Reactor: Model and Simulations, Ind. Eng. Chem. Res. 49 (15) (2010) 6870–6877.

[41] Bayat, M.; Asil, A. G. Efficient In-Situ Water Adsorption for Direct DME Synthesis: Robust Computational Modeling and Multi-Objective Optimization, J. Nat. Gas. Sci. Eng. 83 (2020) 103587.

[42] Gallucci, F.; Paturzo, L.; Basile, A. An Experimental Study of CO_2 Hydrogenation into Methanol Involving a Zeolite Membrane Reactor, Chem. Eng. Process.: Process Intensification 43 (8) (2004) 1029–1036.

[43] Gorbe, J.; Lasobras, J.; Francés, E.; Herguido, J.; Menéndez, M.; Kumakiri, I.; Kita, H. Preliminary Study on the Feasibility of Using a Zeolite A Membrane in a Membrane Reactor for Methanol Production, Sep. Purif. Technol. 200 (2018) 164–168.

[44] Gallucci, F.; Basile, A. A Theoretical Analysis of Methanol Synthesis from CO_2 and H_2 in a Ceramic Membrane Reactor, Int. J. Hydrogen Energy 32 (18) (2007) 5050–5058.

[45] Moon, W. S.; Park, S. B. Design Guide of a Membrane for a Membrane Reactor in Terms of Permeability and Selectivity, J. Memb. Sci. 170 (1) (2000) 43–51.

[46] Struis, R. P. W. J.; Stucki, S. Verification of the Membrane Reactor Concept for the Methanol Synthesis, Appl. Catal. A: General 216 (1) (2001) 117–129.

[47] Khajavi, S.; Jansen, J. C.; Kapteijn, F. Application of a Sodalite Membrane Reactor in Esterification-Coupling Reaction and Separation, Catal. Today 156 (3) (2010) 132–139.

[48] Mardanpour, M. M.; Sadeghi, R.; Ehsani, M. R.; Nasr Esfahany, M. Enhancement of Dimethyl Ether Production with Application of Hydrogen-Permselective Pd-Based Membrane in Fluidized Bed Reactor, J. Ind. Eng. Chem. 18 (3) (2012) 1157–1165.

[49] Choi, S.-W.; Jones, C. W.; Nair, S.; Sholl, D. S.; Moore, J. S.; Liu, Y.; Dixit, R. S.; Pendergast, J. G. Material Properties and Operating Configurations of Membrane Reactors for Propane Dehydrogenation, AIChE J. 61 (3) (2015) 922–935.

[50] Khassin, A. A. Membrane Reactors for the Fischer-Tropsch Synthesis. In Sustainable Strategies for the Upgrading of Natural Gas: Fundamentals, Challenges, and Opportunities; Derouane, E. G., Parmon, V., Lemos, F., Ramôa Ribeiro, F., Eds.; NATO Science Series II: Mathematics, Physics and Chemistry; Springer Netherlands: Dordrecht, 2005 pp. 249–271.

[51] Rohde, M. P.; Schaub, G.; Vente, J. F.; van Veen, H. M. Fischer-Tropsch Synthesis with In-Situ H_20 Removal by a New Hydrophilic Membrane - An Experimental and Modelling Study, Micropor. Mesopor. Mater. 115 (2008) 123–136.

[52] Rohde, M. P.; Schaub, G.; Khajavi, S.; Jansen, J. C.; Kapteijn, F. Fischer–Tropsch Synthesis with in Situ H_2O Removal - Directions of Membrane Development, Micropor. Mesopor. Mater. 115 (1) (2008) 123–136.

[53] Gallucci, F.; Basile, A.; Hai, F. I. Introduction - A Review of Membrane Reactors. In Membranes for Membrane Reactors; Basile, A., Gallucci, F., Eds.; John Wiley & Sons, Ltd: Chichester, UK, 2011, pp. 1–61.

[54] Espinoza, R. L.; du Toit, E.; Santamaria, J.; Menendez, M.; Coronas, J.; Irusta, S. Use of Membranes in Fischer-Tropsch Reactors, Stud. Surf. Sci. Catal. 130 (2000) 389-394.

[55] Hsieh, H. P. Inorganic Membranes for Separation and Reaction; Elsevier Science: New York, 1996.

[56] Najari, S.; Gróf, G.; Saeidi, S. Enhancement of Hydrogenation of CO_2 to Hydrocarbons via In-Situ Water Removal, Int. J. Hydrogen Energy 44 (45) (2019) 24759–24781.

[57] De Falco, M.; Capocelli, M.; Basile, A. Selective Membrane Application for the Industrial One-Step DME Production Process Fed by CO_2 Rich Streams: Modeling and Simulation, Int. J. Hydrogen Energy 42 (10) (2017) 6771–6786.

[58] De Falco, M.; Capocelli, M.; Giannattasio, A. Membrane Reactor for One-Step DME Synthesis Process: Industrial Plant Simulation and Optimization, J. CO_2 Util. 22 (2017) 33–43.

[59] Diban, N.; Urtiaga, A. M.; Ortiz, I.; Ereña, J.; Bilbao, J.; Aguayo, A. T. Influence of the Membrane Properties on the Catalytic Production of Dimethyl Ether with in Situ Water Removal for the Successful Capture of CO_2, Chem. Eng. J. 234 (2013) 140–148.

[60] Diban, N.; Urtiaga, A. M.; Ortiz, I.; Ereña, J.; Bilbao, J.; Aguayo, A. T. Improved Performance of a PBM Reactor for Simultaneous CO_2 Capture and DME Synthesis, Ind. Eng. Chem. Res. 53 (50) (2014) 19479–19487.

[61] Piera, E.; Salomón, M. A.; Coronas, J.; Menéndez, M.; Santamaría, J. Synthesis, Characterization and Separation Properties of a Composite Mordenite/ZSM-5/Chabazite Hydrophilic Membrane, J. Memb. Sci. 149 (1) (1998) 99–114.

[62] Caro, J.; Noack, M.; Kölsch, P.; Schäfer, R. Zeolite Membranes – State of Their Development and Perspective, Micr. Meso. Mat. 38 (1) (2000) 3–24.

[63] Salomón, M. A.; Coronas, J.; Menéndez, M.; Santamaría, J. Synthesis of MTBE in Zeolite Membrane Reactors, Appl. Catal. A: General 200 (1) (2000) 201–210.

[64] Zhu, W.; Gora, L.; van den Berg, A. W. C.; Kapteijn, F.; Jansen, J. C.; Moulijn, J. A. Water Vapour Separation from Permanent Gases by a Zeolite-4A Membrane, J. Memb. Sci. 253 (1) (2005) 57–66.

[65] Rezai, S. A. S.; Lindmark, J.; Andersson, C.; Jareman, F.; Möller, K.; Hedlund, J. Water/Hydrogen/Hexane Multicomponent Selectivity of Thin MFI Membranes with Different Si/Al Ratios, Micr. Meso. Mat. 108 (1) (2008) 136–142.

[66] Coronas, J.; Falconer, J. L.; Noble, R. D. Characterization and Permeation Properties of ZSM-5 Tubular Membranes, AIChE J. 43 (7) (1997) 1797–1812.

[67] Bowen, T. C.; Noble, R. D.; Falconer, J. L. Fundamentals and Applications of Pervaporation through Zeolite Membranes, J. Memb. Sci. 245 (1) (2004) 1–33.

[68] Bernal, M. P.; Piera, E.; Coronas, J.; Menéndez, M.; Santamaría, J. Mordenite and ZSM-5 Hydrophilic Tubular Membranes for the Separation of Gas Phase Mixtures, Catal. Today 56 (1) (2000) 221–227.

[69] Wu, J.; Saito, M.; Takeuchi, M.; Watanabe, T. The Stability of Cu/ZnO-Based Catalysts in Methanol Synthesis from a CO_2-Rich Feed and from a CO-Rich Feed, Appl. Catal. A: General 218 (1) (2001) 235–240.

[70] Lu, W.-Z.; Teng, L.-H.; Xiao, W.-D. Simulation and Experiment Study of Dimethyl Ether Synthesis from Syngas in a Fluidized-Bed Reactor, Chem. Eng. Sci. 59 (22) (2004) 5455–5464.

[71] Kim, H.-J.; Jung, H.; Lee, K.-Y. Effect of Water on Liquid Phase DME Synthesis from Syngas over Hybrid Catalysts Composed of Cu/ZnO/Al_2O_3 and γ-Al_2O_3, Korean J. Chem. Eng. 18 (6) (2001) 838–841.

[72] Ereña, J.; Sierra, I.; Olazar, M.; Gayubo, A. G.; Aguayo, A. T. Deactivation of a CuO−ZnO−Al_2O_3/γ-Al_2O_3 Catalyst in the Synthesis of Dimethyl Ether, Ind. Eng. Chem. Res. 47 (7) (2008) 2238–2247.

[73] Behloul, C. R.; Commenge, J.-M.; Castel, C. Simulation of Reactors under Different Thermal Regimes and Study of the Internal Diffusional Limitation in a Fixed-Bed Reactor for the Direct Synthesis of Dimethyl Ether from a CO_2-Rich Input Mixture and H_2, Ind. Eng. Chem. Res, 60 (4) (2021) 1602–1623

[74] Fernandez Rivas, D.; Boffito, D. C.; Faria-Albanese, J.; Glassey, J.; Afraz, N.; Akse, H.; Boodhoo, Kamelia. V. K.; Bos, R.; Cantin, J.; (Emily) Chiang, Y. W.; Commenge, J.-M.; Dubois, J.-L.; Galli, F.; de Mussy, J. P. G.; Harmsen, J.; Kalra, S.; Keil, F. J.; Morales-Menendez, R.; Navarro-Brull, F. J.; Noël, T.; Ogden, K.; Patience, G. S.; Reay, D.; Santos, R. M.; Smith-Schoettker, A.; Stankiewicz, A. I.; van den Berg, H.; van Gerven, T.; van Gestel,

J.; van der Stelt, M.; van de Ven, M.; Weber, R. S. Process Intensification Education Contributes to Sustainable Development Goals. Part 1, Educ. Chem. Eng. 32 (2020) 1–14.

[75] Keil, F. J. Process Intensification, Rev. Chem. Eng. 34 (2) (2018) 135–200.

[76] Harmsen, J. Process Intensification in the Petrochemicals Industry: Drivers and Hurdles for Commercial Implementation. Chem. Eng. Process.: Process Intensification 49 (1) (2010) 70–73.

[77] Villermaux, J. Génie de la réaction chimique: conception et fonctionnement des réacteurs; Tec & doc, DL 1993: Paris etc., France, 1993.

[78] Nie, Z.; Liu, H.; Liu, D.; Ying, W.; Fang, D. Intrinsic Kinetics of Dimethyl Ether Synthesis from Syngas, J. Nat. Gas. Chem. 14 (1) (2005) 7.

[79] Graaf, G. H.; Sijtsema, P. J. J. M.; Stamhuis, E. J.; Joosten, G. E. H. Chemical Equilibria in Methanol Synthesis, Chem. Eng. Sci. 41 (11) (1986) 2883–2890.

[80] Moradi, G. R.; Ahmadpour, J.; Yaripour, F.; Wang, J. Equilibrium Calculations for Direct Synthesis of Dimethyl Ether from Syngas, Can. J. Chem. Eng. 89 (1) (2011) 108–115.

[81] Schweich, D. Génie de la réaction chimique; Tec & Doc Lavoisier ed.: Paris, 2001.

[82] Mohagheghi, M.; Bakeri, G.; Saeedizad, M. Study of the Effects of External and Internal Diffusion on the Propane Dehydrogenation Reaction over Pt-Sn/Al_2O_3 Catalyst, Chem. Eng. Technol. 30 (12) (2007) 1721–1725.

[83] Commenge, J.-M.; Falk, L.; Corriou, J.-P.; Matlosz, M. Intensification des procédés par microstructuration, Comptes Rendus Physique 5 (5) (2004) 597–608.

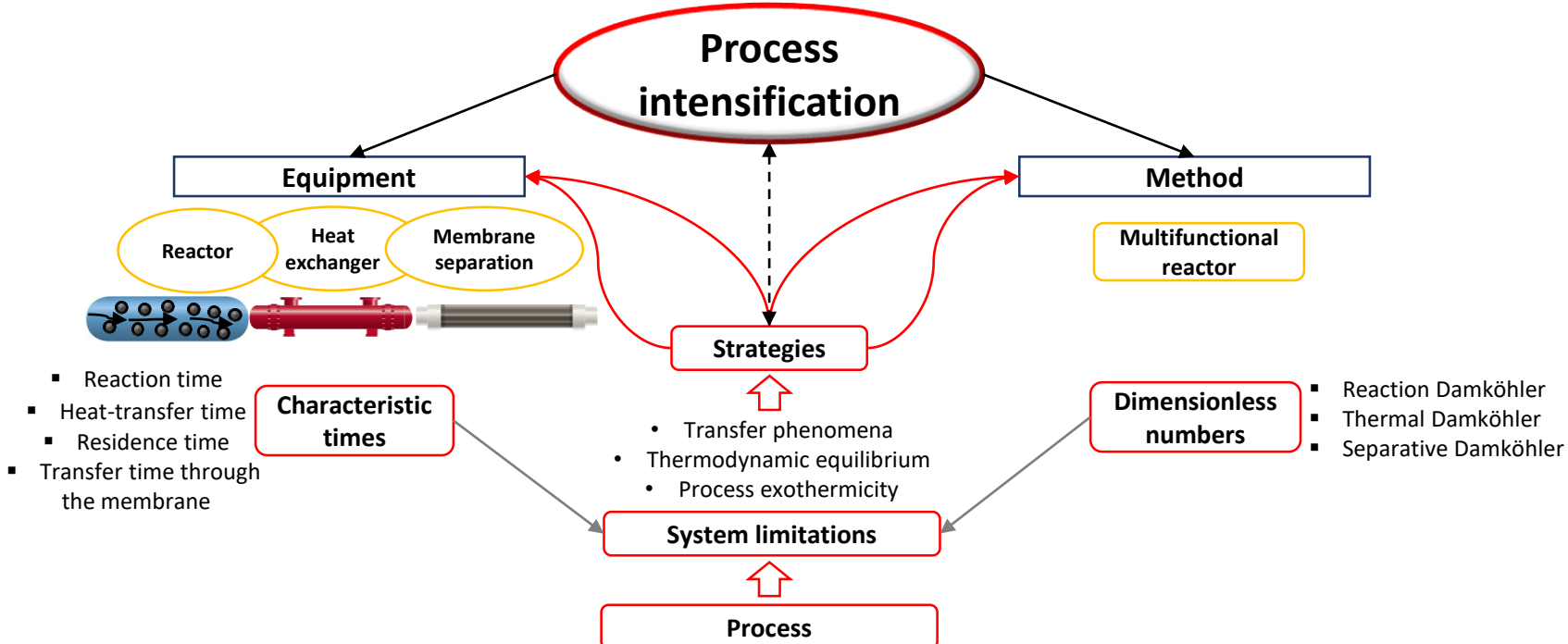
Process intensification
Equipment
Method
Reactor
Heat exchanger
Membrane separation
Multifunctional reactor
Strategies
Reaction time
Heat-transfer time
Residence time
Transfer time through the membrane
Characteristic times
Transfer phenomena
Thermodynamic equilibrium
Process exothermicity
Dimensionless numbers
Reaction Damköhler
Thermal Damköhler
Separative Damköhler
System limitations
Process